

# Augmented Lagrangian methods produce cutting-edge magnetic coils for stellarator fusion reactors

Pedro F. Gil,<sup>1</sup> Alan A. Kaptanoglu,<sup>2</sup> and Eve V. Stenson<sup>1</sup>

<sup>1</sup>*Max-Planck-Institut für Plasmaphysik, 85748 Garching, Germany*

<sup>2</sup>*Courant Institute of Mathematical Sciences, New York University, New York, NY 10012, United States of America*

(Dated: July 18, 2025)

Finding feasible coils for stellarator fusion devices is a crux of realizing this concept for future power plants. The coils must reproduce the physics properties of the target plasma while satisfying myriad engineering constraints. Current efforts struggle to navigate the highly nonconvex optimization landscape and result in suboptimal stellarator coils, and/or they end up spending considerable resources scanning the continuous parameter space. In this work, we present an augmented Lagrangian approach to tackle the ill-posed problem of coil optimization. Our approach yields solutions that out-perform previous Pareto-optimal work and display excellent physics and engineering properties. We conclude by illustrating its effectiveness and versatility by generating coils for five stellarators with very different symmetries and magnetic field shaping. In all cases, we find coil solutions that in various ways outperform published coil sets, including built and operating reactors such as Wendelstein 7-X (W7-X) and the Helically Symmetric eXperiment (HSX).

## I. INTRODUCTION

The stellarator, a toroidal magnetic confinement device, stands as a promising candidate for achieving controlled nuclear fusion. Unlike its axisymmetric counterpart, the tokamak, the stellarator relies on complex, three-dimensional magnetic fields to confine the plasma and therefore does not require the use of induced currents that can lead to plasma instabilities [1–3]. This also allows for steady-state operation, which provides a clear advantage over other technologies to become an energy source. The confining magnetic fields are generated by a system of external coils, the design of which is a critical determinant of the stellarator’s performance and viability. Mathematically, the coils are arbitrary 3D curves in space, and poor optimization of these can easily produce infeasible shapes. Traditionally, stellarator design is subdivided into two stages: stage I, where the plasma boundary shape is optimized, and stage II, where the coil shapes and currents are optimized. This procedure has been used in essentially all previous stellarator designs, including for designing currently operational experiments such as Wendelstein 7-X and HSX [4–6]. This two-stage process allows for stage-I optimization to explore suitable physics properties for fusion reactors by solving the magnetohydrodynamic equations of force balance in fixed-boundary [7–10]. A separate stage-II optimization allows one to focus the optimization on finding feasible coil sets. The optimization of stellarator coils is a magnetostatic ill-posed inverse problem; a multitude of distinct coil configurations can, in principle, generate similar magnetic fields, yet most of these solutions are impractical from an engineering standpoint [11].

Ultimately, coil complexity and requirements for larger build tolerances resulted in delays in the construction and assembly of Wendelstein 7-X and the cancellation of NCSX as it went 70 million dollars above its baseline cost

of 102 million dollars [12, 13]. It has been determined that coil complexity and tolerances accounted for 66% of the cost growth of NCSX. As for Wendelstein 7-X, it took 10 years to build the reactor, suffering from several delays due to lack of engineering capacity, strict margins and tight coil tolerances [5]. Overall it took  $10^6$  hours to complete the 50 modular coils [14].

Historically, the stellarator community has explored various approaches to tackle the challenge of finding simple yet accurate coils. These have ranged from employing stochastic optimization algorithms to prevent getting stuck in local minima and providing robust configurations, performing large-scale scans capable of exploring vast parameter spaces, investigating diverse coil topologies, such as modular, helical or dipole coils, and even optimizing the plasma and the coils simultaneously [15–24]. Despite these varied efforts, finding robust and efficient coil optimization techniques remains a challenge. Currently, various stellarator equilibrium concepts are being investigated also in the industry [25–29]. Most of these concepts take advantage of the various flavors of omnigeneity, which is a magnetic field property allowing for the confinement of collisionless trapped particles [30–33]. This property applies to alpha particles that contain a considerable portion of the energy (3.5 MeV) produced from D-T fusion reactions, essential for plasma heating. Among these flavors being pursued are the quasi-axisymmetric (QA), quasi-helical symmetric (QH) and quasi-isodynamic (QI) configurations [9, 34]. Even with this restriction, there is remarkable freedom in the plasma shape and plasma properties [35, 36]. This represents an additional challenge for the development of a robust coil optimization scheme able to reliably deliver stellarator coil sets independently of the complexity of the magnetic configuration.

The engineering requirements for a fusion reactor include limitations on coil curvature, minimum separation distances between coils, considerations for port access for

diagnostics, heating systems, and maintenance, and so forth. These requirements must compete with the necessity of high field accuracy to reproduce the desired plasma target. The engineering constraints are immense; to see this, consider just the electromagnetic forces on a reactor-scale stellarator design. Lion et al. [25] report that for the Stellaris reactor-scale design, in order to keep the mechanical integrity of the stellarator, steel plates are placed between the coils. These can have thicknesses “between 0.7 m and 1 m and could be forged, with the heaviest plate in this design weighing 58 tons. The inner rings [around the inner side of the stellarator], about 0.7 m thick and weighing about 200 tons each, can also be forged”. It follows that a stellarator coil design that possesses even mildly reduced forces (e.g. 30%) could result in a significantly more economically viable stellarator. Furthermore, it is estimated that the original Stellaris configuration will have anisotropic deformations in the order of 15 mm, arising from electromagnetic loads. This can potentially result in degraded field quality, asymmetries in the heat loads of island divertors, and so forth. The immense force requirements in this example are not unique to Stellaris, rather, they are emblematic of the inevitable challenges of reactor-scale coil design for stellarators.

Finding coil configurations that simultaneously achieve high magnetic field accuracy and adhere to these engineering requirements is a constrained and highly non-convex optimization problem. Nonconvex constraints are very challenging, so in practice this problem is converted into a multi-objective unconstrained optimization problem with weights attached to each objective. These weights are manually tuned to find coil solutions that seem promising, but the values of these weights are hard to choose because they have no physical significance. As many as 10-15 weights are typically used to balance the various engineering tradeoffs.

### A. Contributions of this work

This manuscript implements an augmented Lagrangian method for coil optimization, aimed at tackling this multifaceted challenge. We seek to identify best-to-date stellarator coil designs in terms of the plasma and engineering complexity metrics, while avoiding heuristic and manual tuning of the optimization weights. We prove the value of this new method by finding a substantial set of coil solutions that, in various ways, outperform previously published coil sets. The entirety of this work is implemented and can be reproduced in the SIMSOPT optimization suite [37].

## II. OPTIMIZATION METHOD

Early stellarator coil optimization methods considered a single continuous toroidal surface surrounding the

plasma, called a winding surface, where sheet currents could flow and a current potential was well-defined. A solution for the current potential would be found, and then coils would be “cut” from them. This approach has been used to find the Wendelstein 7-X coils and can be found in codes such as NESCOIL or REGCOIL [38, 39]. More advanced winding surface methods are in development, especially for generating good initial coils and for performing single-stage optimizations [20]. However, such an approach constrains the coils to sit on a single pre-defined toroidal surface and therefore limits the exploration of better coil sets. Recent efforts have introduced the concept of filamentary coils that can be described as a truncated Fourier series, allowing for the adjustment of the Fourier coefficients as the optimization is performed, and avoiding any surface restriction. This is the representation used in this paper within the SIMSOPT software framework, as described below in Cartesian coordinates for the  $i$ -th coil,

$$x^i(\theta) = \sum_{m=0}^M x_{c,m}^i \cos(m\theta) + \sum_{m=1}^M x_{s,m}^i \sin(m\theta), \quad (1)$$

and similarly for  $y^i$  and  $z^i$ . Here,  $\theta$  corresponds to the coil arc length index, the order  $M$  of the decomposition is to be defined by the user. The coefficients  $[x_{c,m}, x_{s,m}, y_{c,m}, y_{s,m}, z_{c,m}, z_{s,m}]$ , along with the currents of the coils, constitute the  $n = N(3(2M + 1) + 1)$  degrees of freedom for  $N$  coils of the optimization problem. Coil optimization can be formulated as an equality and inequality-constrained optimization problem:

$$\begin{aligned} & \underset{\boldsymbol{x}}{\text{minimize}} && f(\boldsymbol{x}) \\ & \text{subject to} && e_j(\boldsymbol{x}) = 0, \quad j \in \mathcal{E} \\ & && g_k(\boldsymbol{x}) \leq 0, \quad k \in \mathcal{I} \end{aligned} \quad (2)$$

Here  $f : \mathbb{R}^n \rightarrow \mathbb{R}$  is the objective function to be minimized,  $e_j : \mathbb{R}^n \rightarrow \mathbb{R}$  and  $g_k : \mathbb{R}^n \rightarrow \mathbb{R}$  correspond to equality and inequality constraints,  $\boldsymbol{x} \in \mathbb{R}^n$  are the degrees of freedom including the Fourier coefficients representing the coil filaments and currents,  $\mathcal{E}$  and  $\mathcal{I}$  are the set of indices for equality constraints and inequality constraints, respectively. Consider  $N_c$  constraints in total. In previous work, the next step is to transform this very challenging constrained optimization into an unconstrained problem by constructing a weighted multi-objective function. This is the mechanism used in SIMSOPT, written in the form:

$$\underset{\boldsymbol{x}}{\text{minimize}} \quad f(\boldsymbol{x}) + \sum_{l=1}^{N_c} \omega_l c_l(\boldsymbol{x}), \quad (3)$$

where  $c_l$  are the various inequality and equality constraints combined and  $\omega_l \in \mathbb{R}$  for  $l = 1, \dots, N_c$  are the weights. Inequality constraints are typically recast to equality constraints by  $g_l \mapsto \max(g_l - g_{\text{target}}, 0)$ , since this quantity vanishes if  $g_l(\boldsymbol{x})$  is below the target value.

As was pointed out in Conlin et al. for plasma optimization [40], the weights  $\omega_l$  have to be set by the user, rarely represent an optimal tradeoff, and therefore have to be adjusted. It is also only possible to satisfy the constraints when  $\omega_l \rightarrow \infty$ . Moreover, in order to circumvent the struggle of weight adjustment, large-scale scans of targets/weights are used, which can be computationally expensive and suffer restriction to local regions of the parameter space. In order to tackle these issues, the following augmented Lagrangian formulism for coil optimization is proposed with the Lagrangian,

$$\mathcal{L}_A(\mathbf{x}, \boldsymbol{\lambda}, \boldsymbol{\mu}) = f(\mathbf{x}) - \boldsymbol{\lambda}^\top \mathbf{c}(\mathbf{x}) + \frac{1}{2} \|\sqrt{\boldsymbol{\mu}} \circ \mathbf{c}(\mathbf{x})\|_2^2, \quad (4)$$

where:

- $\boldsymbol{\lambda} \in \mathbb{R}^{N_c}$  is the vector of Lagrange multipliers.
- $\boldsymbol{\mu} \in \mathbb{R}^{N_c}$  and  $\mu_l > 0$  for all  $l$ , are the penalty parameters.
- $\mathbf{c} : \mathbb{R}^n \rightarrow \mathbb{R}^{N_c}$  is the vector of the original equality constraints.

The term  $\boldsymbol{\lambda}^\top \mathbf{c}(\mathbf{x})$  is the standard Lagrange multiplier term, and  $\frac{1}{2} \|\sqrt{\boldsymbol{\mu}} \circ \mathbf{c}(\mathbf{x})\|_2^2$  is the penalty term defining the Hadamard product between  $\boldsymbol{\mu}$  and  $\mathbf{c}(\mathbf{x})$ . The latter penalizes constraint violations. Note that what previously were user-determined hyperparameters become now Lagrange multipliers that are meant to be updated throughout the optimization, so time consuming manual updates are avoided. Moreover the penalty term prevents the necessity of infinite magnitudes for the  $\omega_l$ , avoiding the two main disadvantages of the previous formalisms. The algorithm employed to steer and update the Lagrange multipliers is inspired from [40–42] and it is here presented and adapted for clarity:

### Augmented Lagrangian Algorithm

---

**Initialize:**  $p = 0$ ,  $\mathbf{x}_0$ ,  $\boldsymbol{\mu}_0 > 0$ ,  $\omega_{tol} > 0$ ,  $\eta_{tol} > 0$ ,  $\tau > 1$

$$\boldsymbol{\lambda}_0 \leftarrow \text{array sampled from uniform distribution in } [0,1]$$

$$\bar{\mu}_0 \leftarrow \text{Average}(\boldsymbol{\mu}_0)$$

$$\omega_0 \leftarrow 1/\bar{\mu}_0$$

$$\eta_0 \leftarrow 1/\bar{\mu}_0^{0.1}$$

**While**  $\|\nabla \mathcal{L}_A(\mathbf{x}_p, \boldsymbol{\lambda}_p, \boldsymbol{\mu}_p)\|_2 > \omega_{tol}$  or  $\|\mathbf{c}(\mathbf{x}_p)\|_\infty > \eta_{tol}$

$$\mathbf{x}_{p+1} \leftarrow \text{argmin}_{\mathbf{x}} \mathcal{L}_A(\mathbf{x}, \boldsymbol{\lambda}_p, \boldsymbol{\mu}_p), \text{ solved to tol. } \omega_p$$

**if**  $\|\mathbf{c}(\mathbf{x}_{p+1}, \boldsymbol{\lambda}_p, \boldsymbol{\mu}_p)\|_\infty < \eta_p$  **then**

$$\boldsymbol{\lambda}_{p+1} \leftarrow \boldsymbol{\lambda}_p - \boldsymbol{\mu}_p \circ \mathbf{c}(\mathbf{x}_{p+1})$$

$$\boldsymbol{\mu}_{p+1} \leftarrow \boldsymbol{\mu}_p$$

$$\omega_{p+1} \leftarrow \max(\omega_p / \bar{\mu}_{p+1}, \omega_{tol})$$

$$\eta_{p+1} \leftarrow \max(\eta_p / \bar{\mu}_{p+1}, \eta_{tol})$$

**else:**

$$\boldsymbol{\lambda}_{p+1} \leftarrow \boldsymbol{\lambda}_p$$

$$\boldsymbol{\mu}_{p+1} \leftarrow \tau \boldsymbol{\mu}_p$$

$$\bar{\mu}_{p+1} \leftarrow \text{Average}(\boldsymbol{\mu}_p)$$

$$\omega_{p+1} \leftarrow \max(1/\bar{\mu}_{p+1}, \omega_{tol})$$

$$\eta_{p+1} \leftarrow \max(1/\bar{\mu}_{p+1}, \eta_{tol})$$

**end if**

```

    p ← p + 1
end while

```

---

Here  $w_{tol}$  is the tolerance of the Lagrangian gradient and  $\eta_{tol}$  is the tolerance for the measure of constraint violation, and together they set the convergence condition. The  $\text{argmin}(\mathcal{L}_A)$  optimization is an internal minimization step where for fixed Lagrange multipliers the local optimizer L-BFGS-B [43] is used, a quasi-Newton method suitable for problems with a high number of degrees of freedom. In the context of SIMSOPT the individual gradients of each constraint function  $c_i(\mathbf{x})$  are calculated using a combination of analytic derivatives and automatic differentiation, where the chain rule is applied using vector-Jacobian products allowing for efficient derivative estimations. As mentioned previously, the goal is to design feasible coils that are able to reproduce exactly the magnetic field of fusion plasmas. Therefore, the main objective of the optimization is to minimize the field error. This is achieved via the normalized squared flux, which is a measure of deviation between the coil magnetic field and the target magnetic surface,

$$f_{SF} = \frac{1}{2} \int_S \frac{|\mathbf{B} \cdot \mathbf{n}|^2}{|B|^2} dS, \quad (5)$$

where  $S$  is the plasma target surface,  $\mathbf{n}$  is its normal vector, and  $\mathbf{B}$  is the magnetic field generated by the coils from the Biot-Savart law,

$$\mathbf{B} = \frac{\mu_0}{4\pi} \sum_{i=1}^N I_i \int_{\Gamma_i} \frac{d\mathbf{l}_i \times \mathbf{r}}{r^3}. \quad (6)$$

Here  $d\mathbf{l}_i$  is the differential arc-length element of the filament,  $\Gamma_i$  is the i-th coil curve and  $\mathbf{r}$  is the distance between the corresponding arc-length element and the evaluation point. When  $f_{SF} = 0$ , the field produced by the stellarator coils is exactly tangential to the desired magnetic plasma surface. If this is achieved, then the plasma MHD equilibrium is ensured. However, computational methods cannot exactly produce  $f_{SF} = 0$  for the entire plasma boundary. This necessity for zero errors seems to imply that  $f_{SF}$  should serve as a candidate for the minimization function  $f$  in Equation 4.

Instead, in this work, the function  $f$  is replaced with a dummy objective function that returns 0, and the squared flux function is moved to the constraints with all the other objectives. This is motivated by the fact that the augmented Lagrangian methods are highly adapted to minimize constraint violation. We also found that for many devices  $f_{SF} \lesssim 10^{-6}$  or so is sufficient for reproducing the plasma properties. In this case, we can convert the squared flux objective to  $\max(f_{SF} - 10^{-6}, 0)^2$ . Once this constraint is satisfied, the algorithm is free to use the extra “slack” to improve engineering constraints, rather than continuing to focus on the squared flux. This is also advantageous because it does not make practical sense to exactly fit  $f_{SF} = 0$ ; there will inevitably be error fields from a host of real-world sources that

will lead to deviations from the desired magnetic fields. Some precisely-quasisymmetric stellarator designs, like the Landreman&Paul QA/QH configurations, have fairly rapid deterioration of the degree of quasisymmetry as  $f_{SF}$  deviates from zero. Nonetheless, these configurations, which have been optimized only for aspect ratio, rotational transform, and quasisymmetry, will not have extremely high degrees of quasisymmetry once they are turned into reactor-designs. In other words, when finite- $\beta$  effects, ideal MHD stability, turbulence reduction, etc. are factored into the optimization problem, the degree of quasisymmetry will decrease and subsequently we expect the sensitivity with respect to errors in  $f_{SF}$  will decrease. *We believe this capability to impose  $f_{SF}$  as an inequality constraint is a substantial advantage of our approach.*

Regarding the remaining coil constraints, we use standard metrics for complexity in the literature [44, 45]:

$$g_{cs} = \sum_{i=1}^N \int_{\Gamma_i} \int_S \max(0, d_0^{cs} - \|\mathbf{r}_i - \mathbf{s}\|_2)^2 dl_i dS, \quad (7a)$$

$$g_{cc} = \sum_{i=1}^N \sum_{j=1}^{i-1} \int_{\Gamma_i} \int_{\Gamma_j} \max(0, d_0^{cc} - \|\mathbf{r}_i - \mathbf{r}_j\|_2)^2 dl_j dl_i, \quad (7b)$$

$$g_l = \frac{1}{2} \left( \max \left( \sum_{i=1}^N L_i - L_0, 0 \right) \right)^2, \quad (7c)$$

$$g_{msc} = \sum_{i=1}^N \frac{1}{2} \int_{\Gamma_i} \max(\kappa - \kappa_0, 0)^2 dl, \quad (7d)$$

$$c_{link}(\Gamma_i, \Gamma_j) = \frac{1}{4\pi} \left| \oint_{\Gamma_i} \oint_{\Gamma_j} \frac{\mathbf{r}_i - \mathbf{r}_j}{|\mathbf{r}_i - \mathbf{r}_j|^3} (\mathbf{dr}_i \times \mathbf{dr}_j) \right|, \quad (7e)$$

$$g_f = \frac{1}{2} \sum_{i=1}^N \left( \int \max(|\mathbf{F}_i(l)| - F_0, 0)^2 dl \right). \quad (7f)$$

$g_{cs}$  is a function penalizing the minimum distance between the last closed flux surface of the plasma and the coils, preventing it from being smaller than  $d_0^{cs}$ . This can allow enough space for the positioning of a tritium-breeding blanket and shielding wall to keep the integrity of the coils and fusion device that can be damaged by high energy neutrons.  $g_{cc}$  restrains the minimum coil-to-coil distance from being smaller than  $d_0^{cc}$ , accounting for finite dimensions of the coils as well as coil assembly and diagnostics. The length of the coils is set by a quadratic penalty that penalizes the sum of length of all the coils if it goes above the threshold  $L_0$ . Longer coils means more expensive superconducting material is required to construct them. The cost function  $g_{msc}$  calculates the  $L_2$  norm of the curvature of a coil and then penalizes the local curvature of the coil if it exceeds the threshold  $\kappa_0$ . Higher curvature coils tend to be more difficult to manufacture and assemble. In order to prevent configurations with interlinked coils, which would be very challenging to build in practice, the Gauss linking number  $c_{link}$  is calculated for each pair and becomes an integer  $\geq 1$  if

they are interlinked. Finally,  $g_f$  minimizes the pointwise self and mutual forces that are above some  $F_0$  threshold representing the tolerances of the superconducting material in the coils. The details for the force estimation can be found in Hurwitz et al. [49]. It has become an increasing necessity to find configurations minimizing the coil-to-coil forces because the required coil currents in a reactor-scale stellarator can reach tens of Mega-Ampere values [20, 45, 50–52]. For the purpose of this work, the estimation of the maximum force per HTS turn is done by dividing the total force value by the number of HTS turns per coil.

In order to determine the relative HTS material requirements for coil sets with varying number of coils per half-field period, for all the following results in this work we assume 200 HTS turns per coil for a reference coilset (e.g. 800 turns total in a four-coil solution) and recalculate the number of turns assuming fixed total current per half-field period (e.g. a three coil solution will be assumed to have 800/3 HTS turns in each coil to keep the total current fixed). This is probably a pessimistic lower bound on the amount of HTS required for solutions with fewer coils, but it also helps to mitigate the forces in these designs.

The interest behind designing stellarators with fewer coils comes from the increased plasma access that is made available on the outboard side. Fewer coils means more space in between coils for placing additional ports for plasma diagnostics, increasing the heating power, and the easing remote maintenance of the device. We find in practice that often the minimum coil-coil and coil-surface distances are higher, meaning less stringent assembly tolerances and more space for a neutron-absorbing blanket. However the price is paid on the quality of the magnetic field and a potentially higher amount of required HTS material.

Lastly, note that while we have avoided the use of manually determined *weights*, we do not get rid of appropriate upper and lower *bounds* on these objectives, as this is typically critical for avoiding undesirable coil solutions such as coils which are all topologically inter-linked. Furthermore, the objectives all have natural upper and lower bounds ( $d_0^{cs}$ ,  $d_0^{cc}$ , ...) for feasibility that are well-motivated by physical and engineering considerations. A summary of natural upper and lower bounds for a reactor-scale stellarator, and their motivation, is provided in Table I.

### III. RESULTS

#### A. Quasi-axisymmetric stellarator

The first goal for this paper is to demonstrate a novel computational framework capable of efficiently reaching, and in fact improving on previously Pareto-optimal solutions. We first consider quasi-axisymmetric stellarators, which are thought to combine the benefits of both stel-

Objective	Bound	Motivation
Squared Flux	$\lesssim 10^{-6}$	Sufficient accuracy to preserve important plasma properties.
Minimum CS distance	$\gtrsim 1.3\text{m}$	Sufficient distance for neutron-absorbing blanket.
Minimum CC distance	$\gtrsim 0.7\text{m}$	Sufficient distance for avoiding coil intersections and assembly difficulties from finite coil build.
Total coil length	$\lesssim 150 - 200\text{m}$	As small as possible to decrease the costs of purchasing superconducting material. But there must be sufficient coil length for coils to be far enough from the plasma to reduce coil-surface distance and improve squared flux.
Max curvature $\kappa$	$\lesssim 1 \text{ m}^{-1}$	Low enough local curvature to simplify geometry and manufacturing costs.
Max MSC	$\lesssim 0.5\text{m}^{-1}$	Similar to the curvature $\kappa$ , the average curvature must remain low so that the coils can be manufactured precisely without extensive cost.
Coil linking #	0	Interlinking coils could greatly increase the complexity of assembly.
Max force	$\lesssim 0.5 \text{ MN/m}$	Max forces must stay within the force tolerances of the HTS material, estimated for industrial REBCO-based cables [46–48].

TABLE I. Rough estimates of upper  $\uparrow$  and lower  $\downarrow$  bounds for engineering metrics of a reactor-scale stellarator design.

larators and tokamaks into one device. This includes the simplicity of the tokamak coils together with the inherent steady-state operation of stellarators. A QA optimized stellarator is in principle also capable of showing neo-classical transport levels comparable to axisymmetric devices as mentioned previously. The start-up company Thea Energy is currently pursuing this concept using dipole coils for their prototype reactor EOS, which will be at first a neutron source [27].

The Landreman&Paul quasi-axisymmetric plasma equilibrium scaled at 1 m major radius found in [9] was chosen in order to be able to compare to the dataset found in [52], and therefore the same optimization set-up is used. This is a plasma configuration with 2-field periods, aspect ratio 6 and rotational transform of 0.42, exceptional confinement properties with a magnetic field error comparable to Earth's magnetic field amplitude.

Kaptanoglu et al [45] performed 8,500 stellarator coil optimizations with five coils per half-field period (hfp) in order to find trade-offs between the magnetic field accuracy that can be achieved with the coils and the Lorentz forces that act on the coils. A similar scan was performed in Hurwitz et al. [52]. From the 8,500 minimization runs on a supercomputer, about 41 defined a Pareto front between the coil forces and the field accuracy which is measured using the surface integrated average of the normal component of the magnetic field to the target surface normalized by its amplitude:  $\langle \mathbf{B} \cdot \mathbf{n} \rangle / \langle B \rangle$ .

In order to filter suitable candidates from the 8,500 configurations, multiple thresholds are applied a-posteriori to be able to determine a valid Pareto-front and remove any undesirable coil solutions that should not be considered (e.g. interlinked coils). The thresholds include a maximum allowed curvature of  $12 \text{ m}^{-1}$ , maximum allowed coil length: 6.5 m, minimum distance between coils and plasma surface: 16.6 cm, minimum distance between coils: 8.3 cm. The number of coil optimizations that were performed in the scans is a testament to the computing power needed in previous methods to achieve optimal devices.

The initial goal of this work is to be able to map this

existing Pareto front. This is done by running our augmented Lagrangian scheme and adjusting the upper linear force threshold to 9, 10, 10.5 and 12 kN/m. Each run takes around 40 minutes on a single CPU core, and is stopped once the algorithm reaches the maximum number of iterations, set to 50 in this case. The quadratic flux also possesses an upper boundary which is on purpose set to low values ( $10^{-15}$ ) to force the optimizer to reach the lowest error configurations. All four configurations are plotted on Figure 1 and they all sit at the Pareto front. These results are calculated with a fixed total length of 25 m; we then try to define a new Pareto front by relaxing this constraint and setting the total length threshold to 30 m. By running 6 different optimizations with the linear force thresholds set to 14, 12, 11, 10, 9.5 and 9 kN/m, it is possible to trace-out a new limit visible in Figure 1 with the black stars. This is a similar class of stellarators as previously, with the main difference that they achieve up to one order of magnitude better field accuracy reaching a  $\langle \mathbf{B} \cdot \mathbf{n} \rangle / \langle B \rangle = 1.97 \times 10^{-5}$  at 14 kN/m.

For the purposes of comparison with the Wechsung et al. [15] solutions in Table II, four-coil configurations are now scaled to reactor size with 5.7T on-axis magnetic field strength and 1.7m minor radius, following ARIES-CS [53]. The total length upper bounds are set to the lengths used for the coils sets in Wechsung's solutions and our solutions are systematically compared. For instance, the 18m total length coils for a 1m major radius design are indicated by L18. Scaled to a reactor, the total coil length is 182m with a 10.13m major radius. As far as we can tell, the Wechsung solutions are essentially Pareto-optimal. Nonetheless, *without tuning the weights*, we can produce a L18 solution that is essentially equivalent to the Wechsung L18 solution; the only significant difference is that the coil-coil distance and max curvature are slightly larger in our solution. Similarly our L20 solution is essentially identical, although arguably improved by reducing the unnecessarily large coil-surface distance and increasing the minimum coil-coil distance by 0.17m. For the L24 solution, we purposely avoid penalizing the force in order to see that only marginal improvements in

Property	3-coil L18	Wechsung L18	L18	Wechsung L20	L20	Wechsung L24	L24
# of coils per hfp ↓	<b>3</b>	4	4	4	4	4	4
$\langle \mathbf{B} \cdot \mathbf{n} \rangle / \langle B \rangle \times 10^{-5} \downarrow$	85.5	91.1	93.7	32	34	<b>4.35</b>	6.0
Max $(\mathbf{B} \cdot \mathbf{n}) / B \times 10^{-4} \downarrow$	28	34	34	13	12	<b>1.6</b>	2.9
Max Force [MN/m] ↓	<b>0.41</b>	0.44	0.43	0.47	0.46	0.55	0.85
Total Length [m] ↓	<b>182</b>	<b>182</b>	<b>182</b>	203	203	243	240
Min CC Distance [m] ↑	<b>1.49</b>	1.34	1.44	1.14	1.31	1.0	1.0
Min CS Distance [m] ↑	2.74	2.75	2.57	2.9	2.71	3.1	<b>3.14</b>
Max $\kappa [m^{-1}] \downarrow$	0.53	<b>0.44</b>	0.5	0.49	0.51	0.49	0.5
Max MSC [ $m^{-1}$ ] ↓	0.05	0.05	0.05	0.05	0.05	0.05	0.05
HTS length [km] ↓	194	<b>146</b>	<b>146</b>	162	162	194	192

TABLE II. Comparison of magnetic field and coil properties for our solutions and the corresponding Wechsung solutions scaled to the ARIES-CS [53] reactor with 5.7T on axis and 1.7m minor radius. Properties that should ideally be lowered (increased) in the design are indicated by ↓ (↑). Here, we assume a fixed total current per half-field period, taking 200 HTS turns per coil for the 4 coil solution as reference, explaining the difference in the max force between the table values and Figure 2.

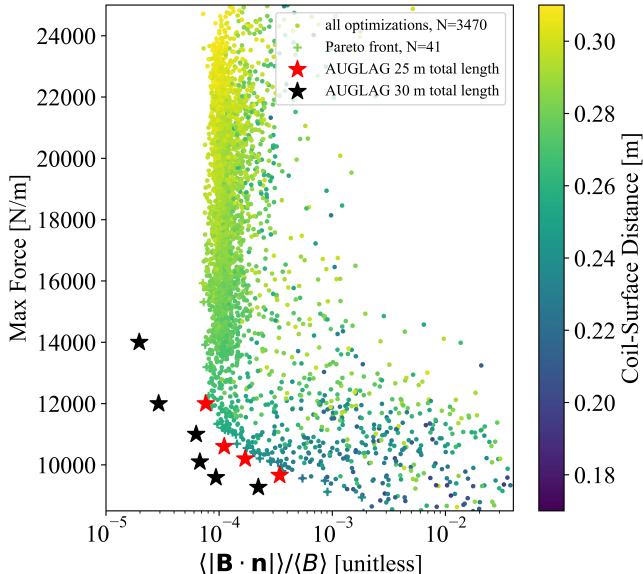


FIG. 1. Scans of QA stellarator configurations from [45] showing trade-offs between coil forces and field accuracy, with red stars placing the new configurations at the found Pareto-front and black ones outlining a new Pareto-front for configurations with larger coil length.

the field accuracy and other metrics are available. At the same time, the max force increases by almost 50% compared to the Wechsung L24 solution. We show this result to illustrate the diminishing returns to “over-optimizing” on the field accuracy.

Lastly, at a given fixed total length, we attempted some three-coil and five-coil solutions. Five-coil solutions were found with comparable or marginally improved performance to the four-coil solutions, so we concluded that the extra coil per half-field period was not worth the inevitable reduction in plasma access. However, assuming that fairly long modular coils can be constructed in practice, an excellent solution was found with 182m total length coil solution with only three coils per hfp. It replicates most of the equivalent (i.e. same total coil

length) four-coil solution complexity metrics while exhibiting better field accuracy and higher coil-coil distances. It can be seen visually in Fig. 2 to provide very good plasma access. These benefits will have to be weighed against the additional coil turns in the three-coil solution that will be necessary to continue avoiding the critical current limits in the superconducting material.

For completeness, the Boozer plot which displays qualitatively the departure from quasisymmetry together with the Poincaré plots showing the nested flux surface structure of the magnetic equilibrium are shown in the Appendix A. Straight lines tell that very low levels of quasisymmetric error are achieved.

Furthermore, the reason why, out of the 8,500 runs performed in previous work only 41 defined a Pareto front, lies in the fact that the adjustment of the weights but also the arbitrary truncation of thresholds modify the stellarator optimization landscape in such a way that it prevents convergence towards good configurations. In contrast, our proposed method takes care of the weight adjustment dynamically throughout the optimization, and informs their update based on the penalty violation of each of the constraints.

## B. Quasi-helical symmetric Stellarator

In a second optimization demonstration, we target the plasma boundary of the Landreman&Paul quasi-helically symmetric (QH) configuration [9]. Like quasi-axisymmetric plasmas, QH equilibria are designed to confined collisionless trapped particles having also reduce alpha-particle losses. The QH configuration is also the only type of quasisymmetry that has been effectively built with the Helically Symmetric eXperiment (HSX)[6], which is explored in Section III E. One of the reasons QH symmetry and more generally quasisymmetric stellarators are of interest for a potential fusion reactor lies in the prediction of shear flows in the plasma, allowing for the suppression of microturbulence [54]. However, a four-field-period QH configuration is considered to be more

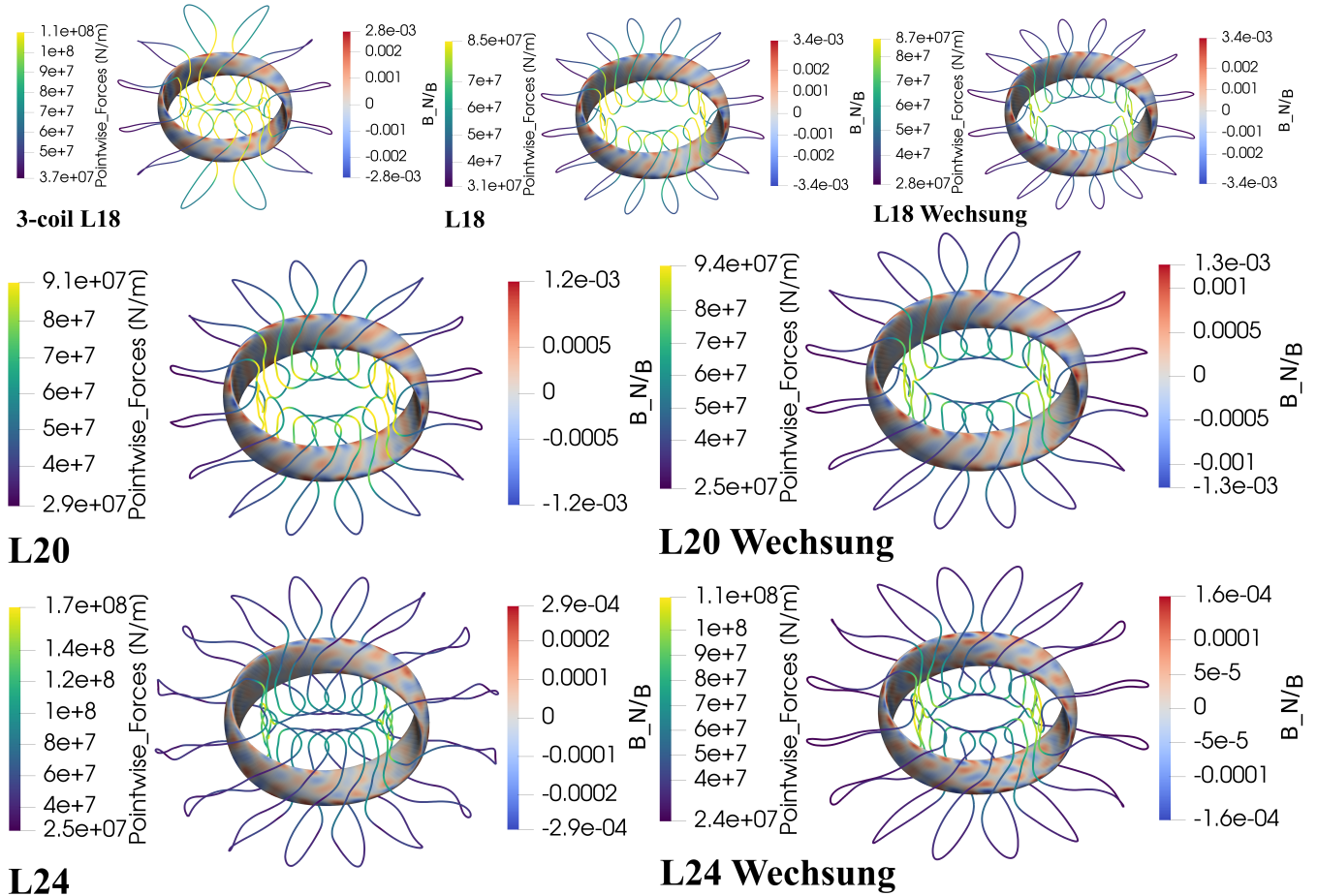


FIG. 2. (Top, left to right) Three-coil solution, four-coil solution, and four-coil Wechsung solution, all with same total coil length. (Middle, left to right) Four coil solution with augmented Lagrangian versus the Wechsung solution obtained at same total coil length. (Bottom, left to right) Same as the middle panel, but with increased total coil length. Forces appear very large because they are reported here before dividing by the number of turns.

demanding from a coil optimization standpoint since the plasma contains more shaping than the QA configuration shown previously. The objective is to reproduce particle confinement properties of this configuration to high enough accuracy. Therefore, the coils here obtained are compared and optimized using the same set-up as in [55], where the main purpose was to obtain a suitable coil configuration at reactor-scale. The major radius of this configurations is approximately 13 m, the aspect ratio is approximately 8 and the average rotational transform is 1.24.

In the original work in Wiedman et al. [55], five coils per hfp were chosen as it was considered that fewer coils did not yield high enough accuracy to reproduce the plasma equilibrium at the coil-to-coil and coil-to-surface distances required. Here, we show that not only it is possible to reproduce a similar configuration as in [55], but it is also possible to reduce the number of coils to four per half field period. The total coil length is also reduced by slightly relaxing other physical requirements. The results for both these optimizations are displayed on

Table III. Together the average field accuracy and maximum field error are comparable to the original work for both the four coil and five coil configurations, the stellarators are shown in Figure 3. Except for 0.2m-reduced minimum coil-coil distance and requiring more HTS material, the four-coil solution is as good, or better, in every engineering metric as the Wiedman solution.

To further verify that these coils generate magnetic fields that fulfill physics requirements, we plot the Boozer plot of the outmost closed magnetic surface together with the Poincaré cross-sections of the equilibrium, shown in Appendix A. As expected the magnetic field amplitude contours appear straight with the low-field regions displaying higher levels of coil ripple than as reported by Wiedman et al., however this is consistent with the fact that the configuration has one less coil per half-field period than previously. It is also possible to reveal the nested structure of the QH equilibrium without any apparent magnetic island chains, capturing the high degree of shaping of the equilibrium.

Confinement of collisionless trapped particles is also

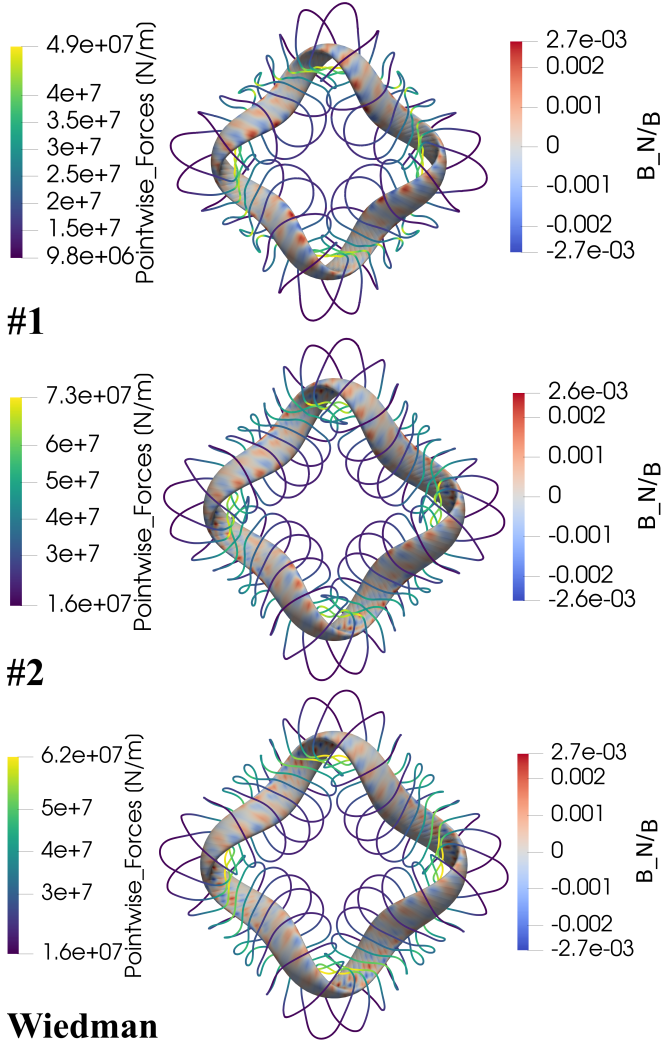


FIG. 3. (Top) The stellarator coil configuration for the 4-coil case (QH4). (Middle) The stellarator coil configuration for the 5-coil case (QH5). (Bottom) Original 5 coil per half-field period QH coilset optimized by Wiedman *et al.* [55]. Forces appear very large because they are reported here before dividing by the number of turns.

strongly suggested by the low quasisymmetric error present in these configurations. Note that this is achieved without necessarily breaching the thresholds and activating the constraints in the optimization. In particular, this is visible in table III for the coil-surface distance (lower bound set to 1.5m) and the maximum curvature (upper bound set to  $1\text{m}^{-1}$ ) for the QH4 and QH5 configurations respectively. This shows that *it is possible to set loose upper and lower bounds and still obtain feasible solutions that do not necessarily achieve the bounds*. In Section III E, we present results in the same spirit as for this configuration but for the fully manufactured and assembled QH HSX stellarator.

Property	#1	#2	Wiedman
# of coils per hfp ↓	<b>4</b>	5	5
$\langle \mathbf{B} \cdot \mathbf{n} \rangle / \langle B \rangle \times 10^{-4} \downarrow$	6.2	6.2	<b>6.1</b>
Max $(\mathbf{B} \cdot \mathbf{n}) / B \times 10^{-3} \downarrow$	2.7	<b>2.6</b>	3.1
Max Force [MN/m] ↓	<b>0.2</b>	0.36	0.31
Total Length [m] ↓	<b>160</b>	177.8	177.8
Min CS Distance [m] ↑	<b>1.91</b>	1.59	1.62
Min CC Distance [m] ↑	0.8	<b>1.09</b>	<b>1.09</b>
Max $\kappa [\text{m}^{-1}] \downarrow$	1	<b>0.77</b>	0.81
Max MSC [ $\text{m}^{-1}$ ] ↓	0.1	0.08	<b>0.079</b>
Quasisym. Error $\times 10^{-3} \downarrow$	5.2	2.3	<b>2.2</b>
HTS length [km] ↓	320	284.5	284.5

TABLE III. Comparison of coil properties for the three different QH configurations, assuming 200 turns per coil for the max force calculations. Properties that should ideally be lowered (increased) in the design are indicated by ↓ (↑).

### C. Stellaris: a Stable Quasi-Isodynamic Stellarator (SQuID)

A third demonstration of the improvement brought by our method is shown on a Stable Quasi-Isodynamic Design (SQuID) stellarator configuration [34] that was recently published by the fusion start-up Proxima Fusion [25] to serve as prototype for a fusion power plant. The interest behind this class of stellarators lies in their physics properties and recent optimization reported in [34], where they appear MHD stable, as a consequence the maximum- $\mathcal{J}$  property described in [56, 57]. This property is also predicted to mitigate turbulence from the trapped electron mode (TEM) [3, 58, 59]. The same class of stellarators is being pursued by other companies such as Type One Energy [26]. Moreover, SQuIDs display low small collisional thermal transport, bootstrap current, and fast-ion losses, which can have a great impact on plasma heating, stability and divertor operation [3, 57, 60]. Finally, there is also evidence suggesting that ITG turbulent heat fluxes of SQuIDs are below that of the W7-X stellarator [34]. However, for past QI configurations it has been challenging to find buildable and accurate coils such as W7-X. On top of that, fine-tailored fieldline curvature imposing the maximum- $\mathcal{J}$  property or MHD stability render the task even more complex. Proxima Fusion published a four field-period SQuID configuration with major radius 12.7m, minor radius 1.3m, a plasma volume of  $425\text{m}^3$  (about half the volume of ITER), an axis averaged magnetic strength of 9T, and is supposed to deliver 2700 MW of peak fusion power. Therefore, the coilset found by Proxima consists of six coils for half-field period. While this allows for more field accuracy, it also comes at the cost that by accounting for the finite-dimensions of the winding pack, the minimum casing-to-casing distance reaches 11.4 mm and assuming 200 turns per coil, peak HTS turn linear force on the filamentary coils is of 0.9 MN/m. This value is at the peak material force tolerances and limits the possibility for structural supports. These very tight engineering

constraints are typical for reactor-scale stellarators.

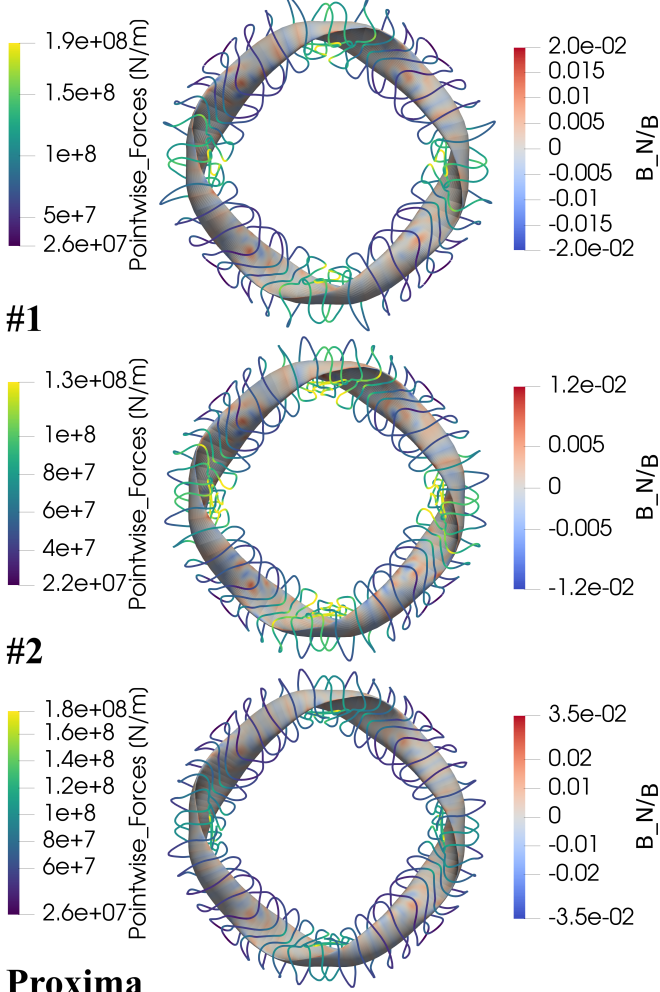


FIG. 4. (Top) First possible configuration for the Stellaris SQuID with 5 coils per half-field period, same field errors. (Middle) Second possible configuration for the Stellaris SQuID with similar parameters but forces are reduced by 29%. (Bottom) Proxima's configuration with 6 coils per hfp, recently published in [25]. Forces appear very large because they are reported here before dividing by the number of turns.

Here two alternative configurations are presented, one with 5 coils and the other with 6 coils per half-field period. In the former case, setting similar thresholds as the characteristics of Proxima's coilset except for the inter-coil distance, yields a configuration that improves on the magnetic field error average by 25%, as well as giving an additional 13 cm of space between coils which allows for better handling of eventual inaccuracies from manufacturing, assembly, thermal contraction or magnetic forces which appear 5% larger. The coilset is displayed on Figure 4. The main parameters are summarized on IV. Taking 200 turns per coil in the 6-coil solutions as reference and fixed total current per half-field period, it is possible to extrapolate the amount of HTS length required for the 2 solutions. While the two solutions come at a slightly

higher cost of HTS tape, these configurations can enable extra access to the plasma, and facilitate reactor maintenance, which is a cost driver. Moreover, the 6 coil case improves on both the 5 coil configuration and Proxima's coils with a field error that is cut by around half, linear forces on the HTS turns that are 29% lower, similar distances between coils and between the plasma surface and the conductor as Proxima. Note that this is however a conservative estimate of the amount of HTS required as it assumes that the tape is always operated at the limit of arbitrarily set engineering requirements for the critical current.

In order to achieve the reduced force configuration, the curvature and length curvatures constraints were relaxed, allowing the total length of the conductors to reach 145 m. The corresponding Boozer plots which serve as a verification for the departure from the target isodynamicity are shown in Appendix A. As shown in Table IV, the Stel-

Property	#1	#2	Proxima
# of coils per hfp ↓	<b>5</b>	6	6
$\langle \mathbf{B} \cdot \mathbf{n} \rangle / \langle B \rangle \times 10^{-3} \downarrow$	3.0	<b>2.3</b>	4.0
Max $(\mathbf{B} \cdot \mathbf{n}) / B \times 10^{-2} \downarrow$	2.2	<b>1.6</b>	3.5
Max Force [MN/m] ↓	0.79	<b>0.64</b>	0.9
Total Length [m] ↓	<b>130</b>	145	138
Min CC Distance [m] ↑	<b>0.8</b>	0.7	0.67
Min CS Distance [m] ↑	<b>1.38</b>	1.3	1.37
Max $\kappa [m^{-1}] \downarrow$	<b>1.57</b>	1.6	<b>1.57</b>
Max MSC [ $m^{-1}$ ] ↓	<b>0.3</b>	0.35	0.34
HTS Length [km] ↓	250	232	<b>221</b>

TABLE IV. Comparison of magnetic field and coil properties for the three different Stellaris configurations. #1 and #2 are results from this work, the Proxima configuration was optimized by the start-up Proxima Fusion. Forces were scaled by assuming 200 turns per coil in the six-coil solution and fixed total coil current per half-field period.

laris configuration is improved in essentially all aspects by the two different coil solutions found here, except potentially for the amount of HTS required. Nonetheless, final decisions about coil and HTS stack design require full finite-element modeling of the coils and structural supports beyond the scope of this work.

#### D. Wendelstein 7-X (W7-X)

So far the configurations described correspond to devices that have been conceptualized but not yet built. In this and the next sections, we show that it is possible to even improve the coil designs of stellarators that have been fully manufactured and assembled and already delivered experimental results. The predecessor of Wendelstein 7-X, Wendelstein 7-AS, was the first stellarator to successfully demonstrate that the two stage approach to stellarator design, as previously described, is able to generate a feasible reactor [11]. In order to bring forward the stellarator program the main goals of W7-X were to demonstrate the generation of nested magnetic

surfaces with modular superconducting coils, enhanced fast-particle confinement, reduced parallel currents, minimal neoclassical transport at low collisionality, and MHD stability up to an average plasma beta of 5% [61]. Wendelstein 7-X is currently the largest operating stellarator in the world, being at the forefront of stellarator research and fusion science generally. The first experimental campaign was performed in 2015, using NbTi superconducting coils to generate a quasi-isodynamic magnetic field with 3T on axis. As mentioned in the introduction, the W7-X manufacturing and assembly process presented various delays due to tight coil tolerances. In practice this meant that many of the manufactured coils were discarded as they did not meet the requirements, resulting in additional costs.

Three different configurations are presented as options for W7-X in Figure 5. As is illustrated in Table V, all

Property	#1	#2	#3	W7-X
# of coils per hfp ↓	4	5	5	5
$\langle \mathbf{B} \cdot \mathbf{n} \rangle / \langle B \rangle \times 10^{-3} \downarrow$	10	6.7	<b>6.6</b>	29
Max $(\mathbf{B} \cdot \mathbf{n} / B) \times 10^{-2} \downarrow$	5.5	<b>4.1</b>	4.2	11
Max Force [kN/m] ↓	<b>15</b>	<b>15</b>	19	19
Total Length [m] ↓	<b>38</b>	45	43	42.6
Min CC Distance [m] ↑	<b>0.3</b>	0.27	0.26	0.28
Min CS Distance [m] ↑	0.32	0.3	0.34	<b>0.37</b>
Max $\kappa [m^{-1}] \downarrow$	2.51	<b>2.0</b>	<b>2.0</b>	2.56
Max MSC [ $m^{-1}$ ] ↓	<b>1.5</b>	<b>1.5</b>	<b>1.5</b>	1.96
HTS Length [km] ↓	95	90	86	<b>85.2</b>

TABLE V. Comparison of magnetic field and coil properties for the four different W7-X configurations. #1, #2 and #3 are results from this work, the W7-X configuration was taken from the original CAD files and adapted as single filaments for the W7-X standard configuration (without additional planar coils). Here the max force and HTS length are computed with 200 HTS turns per coil using the five-coil solution and fixed total current per half-field period.

the configurations are optimized to possess lower curvatures than the original W7-X coilset. The results are visible in the coils shown in Figure 5, as all the newly optimized coils appear smoother and with less local curvature than the W7-X ones. Note that all configurations possess comparable lengths to the W7-X coils. This freedom is purposely imposed for this study, as the goal is to explore options to the current W7-X reactor coils and not to replicate it.

Configuration #1 presents substantial advantages over the original W7-X coilset; the full reactor requires 40 coils instead of 50, but still provides better field accuracy, reduced total coil length, increased minimum coil-coil distance, and reduced curvatures. In every metric it is improved over the original design, except for a 5cm reduced minimum plasma-coil distance. Access to the plasma is substantially increased, as can be seen visually in Fig. 5. The reduced number of coils can help to drive costs down by reducing material, reducing assembly difficulties, and increasing the amount of plasma access for diagnostics, which has become a bottleneck in the operation of W7-X.

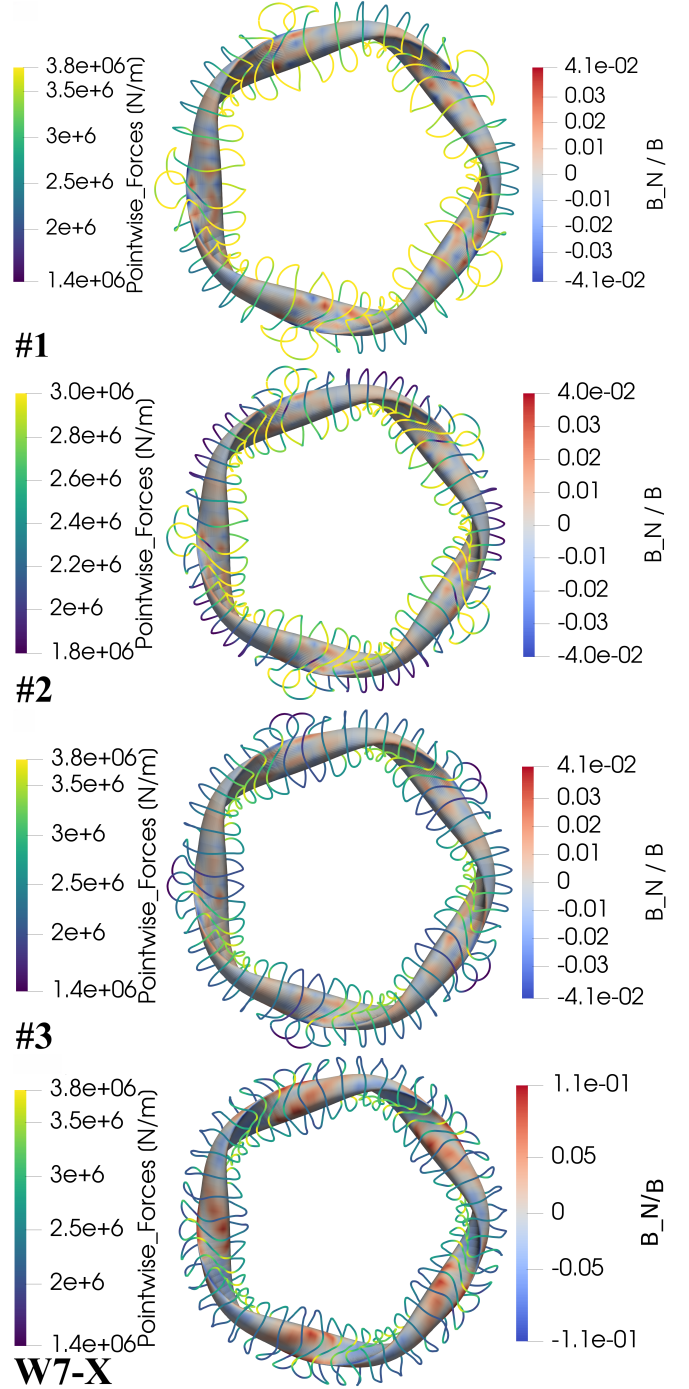


FIG. 5. (#1) First alternative configuration for the W7-X stellarator with 5 coils per half-field period, improved field errors, simpler coils. (#2) Second alternative coilset for the W7-X stellarator with improved field accuracy, 20% less forces, longer coils, but lower curvature. (#3) Third alternative coilset for W7-X with improved field error, similar coil length, same forces and simpler coils. (#4) Original W7-X coilset extracted from the CAD design with 5 coils per half-field period. Forces appear very large because they are reported here before dividing by the number of turns.

Configuration #2 is targeted to reduce the electromag-

netic forces compared to the original design. By allowing only an increase of 5% of the total coil length, slightly closer coils to each other and to the plasma, it is possible to achieve a reduction of about 20% of the force load on the support structure and coils of W7-X. Note that it has been reported by Pedersen et al. [62] that the rotational transform profile and island chain structure are modified due to deformations in the coil shapes resulting from increasing electromagnetic forces. Additionally this new configuration comes with an improvement of about an order of magnitude in field accuracy. Configuration #3 is also an exciting find. With very tiny changes of 0.4m more total coil length, 0.02m reduction to minimum coil-coil distance, and 0.03m reduction to minimum coil-surface distance, the squared flux and curvatures are dramatically improved, without change to the max forces.

The degree of omnigeneity for all coil sets displayed by the magnetic field strength contours is plotted in Appendix A. All W7-X alternatives show contours following the target field. As shown in Figure 5, the #2 and #3 alternatives possess four visibly simple coils out of five with only one coil type standing out as longer. It also appears that lower overall forces can be achieved by relaxing the length constraint on an individual coil type. To our current knowledge and given the current parameters of the W7-X coils displayed in Table V, any of these three alternatives of W7-X could be considered as candidates for a W7-X-style research reactor.

### E. Helically Symmetric eXperiment (HSX)

The Helically Symmetric eXperiment (HSX) is a stellarator located at the University of Wisconsin in Madison. The device began operation in 1999, and was and still is the only device in the world with a quasi-helical stellarator field. It is a four field period stellarator with 48 copper coils, around 1T on axis and major radius of 1.4m. HSX was designed to demonstrate reduced direct orbit losses, Mercier stability, and reduced neoclassical transport. Due to its rotational transform of 1.05 on axis and quasi-helical field, its neoclassical confinement is similar to a  $q = 1/3$  tokamak [6]. It has also managed to demonstrate reduced flow damping and reduced electron heat transport [63, 64]. Unlike the QH stellarator equilibrium shown in Section III B which was optimized for low quasisymmetric error throughout the volume, HSX was only optimized for quasisymmetry on the last closed flux surface because at the time no robust optimization methods had been developed yet. Similarly to W7-X, HSX coils were obtained using a winding surface method, which yielded six coils per half field period with high curvatures. From the twisted filaments, a copper winding pack was constructed for the final reactor, these are shown in Figure 6. The procedure in this section does not aim at improving the forces, since the force requirements become much more stringent at reactor-scale. Given the

smaller dimensions and relatively low magnetic fields of this device, we focus instead on finding simpler coils that are easier to manufacture. We propose three different configurations with four, five, and six coils per half-field period, summarized in Table VI. As expected, the average field error progressively increases with decreasing number of coils. This is consistent with the results from the previous QH, Stellaris and W7-X configurations.

Property	#1	#2	#3	HSX
# of coils per hfp ↓	<b>4</b>	5	6	6
$\langle \mathbf{B} \cdot \mathbf{n} \rangle / \langle B \rangle \times 10^{-3}$ ↓	11	7.5	<b>5.3</b>	5.8
Max $(\mathbf{B} \cdot \mathbf{n})/B \times 10^{-2}$ ↓	4.7	4.2	<b>2.2</b>	2.5
Max Force [kN/m] ↓	0.7	0.88	0.7	<b>0.6</b>
Total Length [m] ↓	<b>10.0</b>	12.1	13.4	13.4
Min CC Distance [m] ↑	<b>0.10</b>	<b>0.10</b>	0.09	0.09
Min CS Distance [m] ↑	<b>0.15</b>	0.13	0.11	0.14
Max $\kappa [m^{-1}]$ ↓	9.7	12	<b>8</b>	12.34
Max MSC [ $m^{-1}$ ] ↓	<b>25</b>	30	30.0	45.1
HTS length [km] ↓	24	23.2	<b>21.4</b>	<b>21.4</b>

TABLE VI. Comparison of magnetic field and coil properties for the four different HSX configurations. #1, #2 and #3 are results from this work, the HSX configuration was taken from the original CAD files and adapted as single filaments for the HSX standard Quasi-Helical Symmetry QHS configuration. Here the max force is the force on 200 turns of HTS per coil in the reference six-coil solution.

The three proposed configurations are mostly characterized by their reduction in curvature, which can be understood as a proxy for coil complexity. The reduction in mean squared curvature reaches 45% in configuration #1, and absolute normal curvature is decreased by 35% in configuration #3. Despite configuration #3 exhibiting the same number of coils per hfp, it manages to improve on the field accuracy while having simpler coils, the same clearance inbetween coils, and losing only 3 cm in the coil-to-surface distance. The forces are generally increased in all the optimized configurations, as they are not a target. It remains the sole aspect where the original HSX design is better.

Configuration #1 is an exemplary solution. Configuration #1 has reduced by two the number of coils per half field period. This level of coil reduction has not been tried in previous sections, as it is often expected that field accuracy will not be precise enough with so few coils per hfp. Amazingly, and despite the fewer coils per hfp, configuration #1 has reasonable field accuracy, and, compared with the original six-coil design, improved minimum coil-coil and coil-surface distances, lower curvatures, and achieves all of these improvements with 25% less total coil length. Despite the factor of two increase in field error compared to the original design, the magnetic field contours plotted in 11 still display comparable accuracy to the other candidates. As previously mentioned, less coils are of particular interest in a research scale reactors where additional diagnostics are usually designed throughout the operation time and need space for new ports. The additional space in between coils on the out-

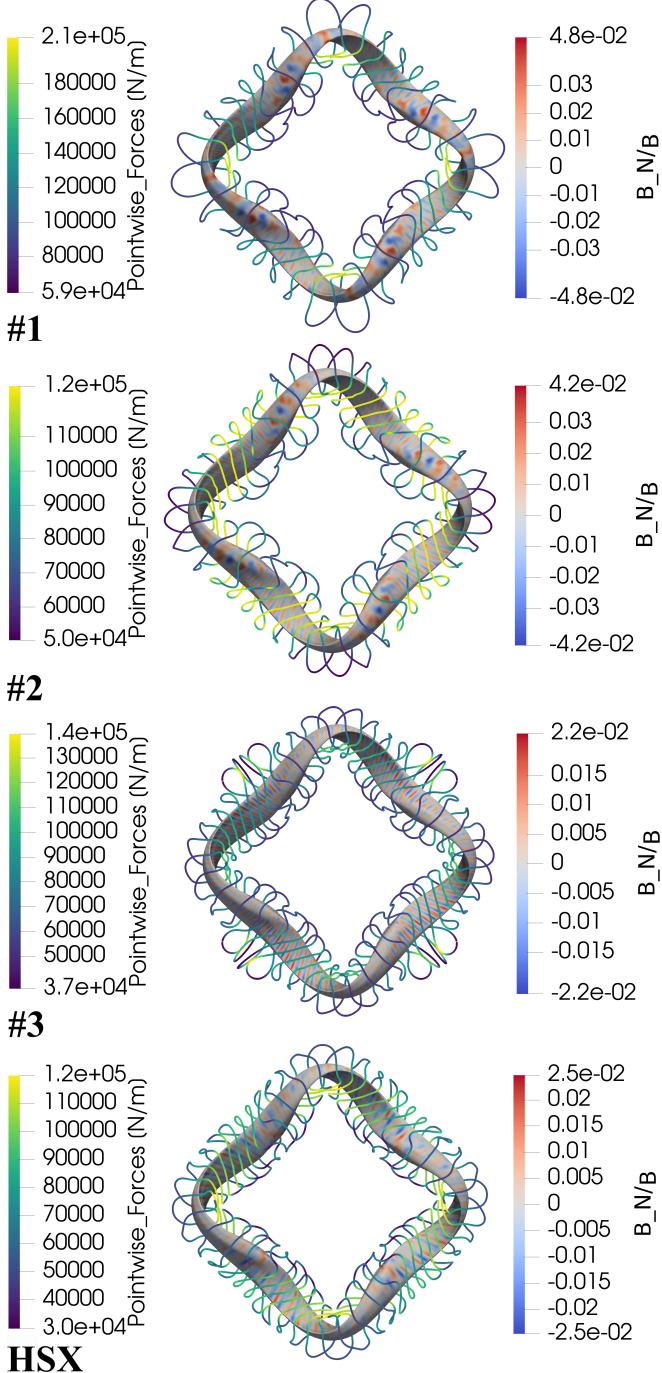


FIG. 6. (#1) First alternative configuration for the HSX stellarator with 4 coils per half-field period, simpler coils, improved coil-to-surface and intercoil distance. (#2) Second alternative coilset for the HSX stellarator with 5 coils per half-field period and simpler coils. (#3) Third alternative coilset for HSX with improved field error, similar coil length, and considerably simpler coils. (#4) Original HSX coil design with 6 coils per half-field period. Forces appear very large because they are reported here before dividing by the number of turns.

board side is noticeable on Figure 6. Less coils also means

less machining time and workforce required in the case of HSX as the coils are made out of copper and usually require the operation of CNC-milling or other heavy machinery devices. This can directly translate to reduced costs, which is often a limiting factor in university scale reactors and more generally in any type of reactor.

#### IV. CONCLUSION

In this work, we have introduced and validated a novel optimization methodology that fundamentally advances the state-of-the-art in stellarator coil design. The challenge of designing magnetic coils for a fusion reactor has long been characterized by difficult tradeoffs between achieving the precise magnetic field geometry required for plasma confinement and satisfying practical engineering constraints. Existing methods often lead to computationally intensive searches through vast parameter spaces, with no guarantee of arriving at a viable, let alone optimal, solution. Our approach confronts this challenge, establishing a robust and computationally efficient pathway for generating coil sets that are not only consistent with desired plasma equilibria but are also potentially manufacturable and meet the stringent requirements for reactor integration. Our methodology was successfully implemented and tested using the SIMSOPT framework.

By applying an augmented Lagrangian approach to coil optimization, it was possible to address three critical issues: (1) the automated adjustment of weights for satisfying the constraints in a non-convex optimization problem, (2) the need for large computational resources and (3) optimally satisfying the tradeoff between low field errors and engineering constraints. In order to showcase the high performance of our method, five very different stellarator equilibria were considered, including quasi-axisymmetric, quasi-helically symmetric and quasi-isodynamic designs. New alternative coil sets were found for two operating stellarators, Wendelstein 7-X and HSX. This demonstrates the versatility of this method in order to generate cutting-edge coils independently of the plasma boundary. The quasi-axisymmetric design illustrated one of the main points of this work: the ability to perform single-optimization runs that achieve known Pareto-optimal solutions. By relaxing various constraints of the coil configurations, we were able to access new Pareto-boundaries. The automated weight tuning and reliance on upper and lower bounds allows one to specify loose parameter space bounds, increasing the space of possible solutions.

All optimizations were performed on an Intel core i7-12650H laptop on 4 cores for Python multi-threading and on 1 core for the evaluations of the functions and gradients. Future work includes accelerating the design of stellarator fusion reactors using modular coils, application to dipole coil arrays, incorporation into single-stage optimization efforts, and further algorithmic improvements.

## ACKNOWLEDGMENTS

This work was supported through grants from the Simons Foundation under award 560651 and from the Helmholtz Association Young Investigators Group program as project VH-NG-1430. We thank Jorrit Lion, Gabriel Plunk, Alan Goodman, Matt Landreman, and Benedikt Geiger for sharing plasma boundary configuration files, and Rory Conlin, Paul Huslage, David Bindel

and Tom Simpson for useful discussions.

## Appendix A: Equilibria verification

This section prevents post-processing illustrations demonstrating that the physics properties of the plasma are well-conserved for the coil solutions identified in this work. Fig. 7 illustrates Boozer and Poincaré plots for a Landreman&Paul QA coil solution, and similarly for Landreman&Paul QH in Fig. 8, Stellaris in Fig. 9, W7-X in Fig. 10, and HSX in Fig. 11.

- 
- [1] F. C. Schuller, Disruptions in tokamaks, *Plasma Physics and Controlled Fusion* **37**, A135 (1995).
- [2] G. Jahns, M. Soler, B. Waddell, J. Callen, and H. Hicks, Internal disruptions in tokamaks, *Nuclear Fusion* **18**, 609 (1978).
- [3] P. Helander, C. D. Beidler, T. M. Bird, M. Drevlak, Y. Feng, R. Hatzky, F. Jenko, R. Kleiber, J. H. E. Proll, Y. Turkin, and P. Xanthopoulos, Stellarator and tokamak plasmas: a comparison, *Plasma Physics and Controlled Fusion* **54**, 124009 (2012).
- [4] G. Grieger, W. Lotz, P. Merkel, J. Nührenberg, J. Sapper, E. Strumberger, H. Wobig, R. Burhenn, V. Erckmann, U. Gasparino, L. Giannone, H. J. Hartfuss, R. Jaenicke, G. Kühner, H. Ringler, A. Weller, F. Wagner, the W7-X Team, and the W7-AS Team, Physics optimization of stellarators, *Physics of Fluids B: Plasma Physics* **4**, 2081 (1992), [https://pubs.aip.org/aip/pfb/article-pdf/4/7/2081/12264911/2081\\_1\\_online.pdf](https://pubs.aip.org/aip/pfb/article-pdf/4/7/2081/12264911/2081_1_online.pdf).
- [5] T. Klinger, C. Baylard, C. Beidler, J. Boscary, H. Bosch, A. Dinklage, D. Hartmann, P. Helander, H. Maßberg, A. Peacock, T. Pedersen, T. Rummel, F. Schauer, L. Wegener, and R. Wolf, Towards assembly completion and preparation of experimental campaigns of Wendelstein 7-X in the perspective of a path to a stellarator fusion power plant, *Fusion Engineering and Design* **88**, 461 (2013), proceedings of the 27th Symposium On Fusion Technology (SOFT-27); Liège, Belgium, September 24–28, 2012.
- [6] F. Anderson, A. Almagri, D. Anderson, P. Matthews, J. Talmadge, and J. Shohet, Helically symmetric experiment, (hsx) goals, design and status, *Fusion Technology* **27**, p. 273–277. (1995).
- [7] S. P. Hirshman and J. C. Whitson, Steepest-descent moment method for three-dimensional magnetohydrodynamic equilibria, *The Physics of Fluids* **26**, 3553 (1983), [https://pubs.aip.org/aip/pfl/article-pdf/26/12/3553/12590952/3553\\_1\\_online.pdf](https://pubs.aip.org/aip/pfl/article-pdf/26/12/3553/12590952/3553_1_online.pdf).
- [8] J. Nührenberg and R. Zille, Quasi-helically symmetric toroidal stellarators, *Physics Letters A* **129**, 113 (1988).
- [9] M. Landreman and E. Paul, Magnetic fields with precise quasisymmetry for plasma confinement, *Phys. Rev. Lett.* **128**, 035001 (2022).
- [10] D. W. Dutt and E. Kolemen, Desc: A stellarator equilibrium solver, *Physics of Plasmas* **27**, 102513 (2020), [https://pubs.aip.org/aip/pop/article-pdf/10.1063/5.0020743/15926767/102513\\_1\\_online.pdf](https://pubs.aip.org/aip/pop/article-pdf/10.1063/5.0020743/15926767/102513_1_online.pdf).
- [11] L.-M. Imbert-Gérard, E. J. Paul, and A. M. Wright, *An Introduction to Stellarators: From Magnetic Fields to Symmetries and Optimization* (Society for Industrial and Applied Mathematics, Philadelphia, PA, 2024) <https://epubs.siam.org/doi/pdf/10.1137/1.9781611978223>.
- [12] V. Erckmann, H.-J. Hartfuss, M. Kick, H. Renner, J. Sapper, F. Schauer, E. Speth, F. Wesner, F. Wagner, M. Wanner, A. Weller, and H. Wobig, The w7-x project: scientific basis and technical realization, in *17th IEEE/NPSS Symposium Fusion Engineering (Cat. No.97CH36131)*, Vol. 1 (1997) pp. 40–48 vol.1.
- [13] R. Strykowsky, T. Brown, J. Chrzanowski, M. Cole, P. Heitzenroeder, G. Neilson, D. Rej, and M. Viol, Engineering cost & schedule lessons learned on ncsx, in *2009 23rd IEEE/NPSS Symposium on Fusion Engineering* (2009) pp. 1–4.
- [14] H.-S. Bosch, R. Brakel, T. Braeuer, V. Bykov, P. van Eeten, J.-H. Feist, F. Füllenbach, M. Gasparotto, H. Grote, T. Klinger, H. Laqua, M. Nagel, D. Naujoks, M. Otte, K. Risze, T. Rummel, J. Schacht, A. Spring, T. Sunn Pedersen, R. Vilbrandt, L. Wegener, A. Werner, R. Wolf, J. Baldzuhn, C. Biedermann, H. Braune, R. Burhenn, M. Hirsch, U. Höfel, J. Knauer, P. Kornejew, S. Marsen, T. Stange, H. Trimino Mora, and W.-X. Team, Final integration, commissioning and start of the Wendelstein 7-X stellarator operation, *Nuclear Fusion* **57**, 116015 (2017).
- [15] F. Wechsung, A. Giuliani, M. Landreman, A. Cerfon, and G. Stadler, Single-stage gradient-based stellarator coil design: stochastic optimization, *Nuclear Fusion* **62**, 076034 (2022).
- [16] A. Giuliani, Direct stellarator coil design using global optimization: application to a comprehensive exploration of quasi-axisymmetric devices, *Journal of Plasma Physics* **90**, 905900303 (2024).
- [17] R. Wu, T. Kruger, and C. Swanson, Planar coil optimization for the Eos stellarator using sparse regression, *Plasma Physics and Controlled Fusion* **67**, 035019 (2025).
- [18] R. Jorge, A. Giuliani, and J. Loizu, Simplified and flexible coils for stellarators using single-stage optimization, *Physics of Plasmas* **31**, 112501 (2024).
- [19] Y. Suzuki, J. Huang, N. Wang, and Y. Ding, Design of simple stellarator using tilted toroidal field coils, *Fusion Engineering and Design* **173**, 112843 (2021).

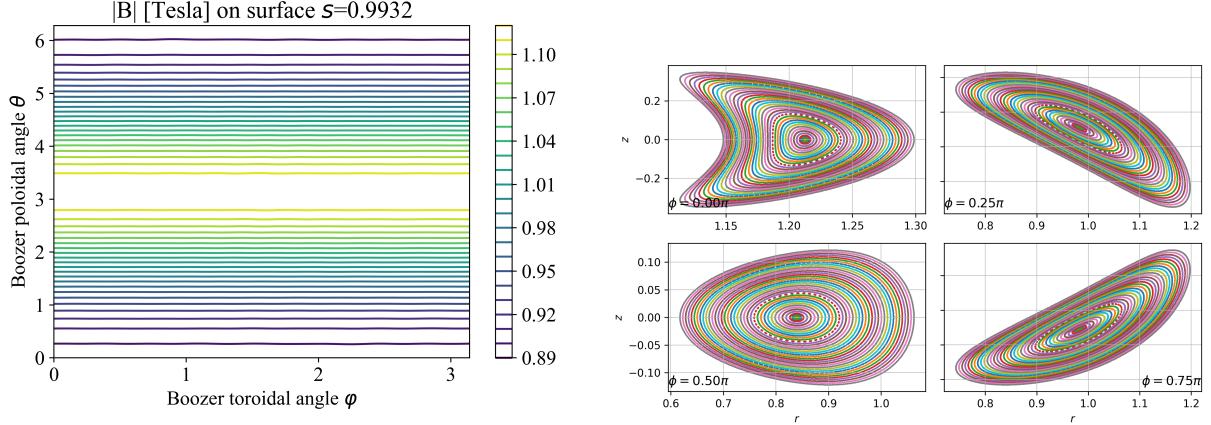


FIG. 7. (Left) Boozer plot of the AL25 configuration showing the quality of the quasi-symmetry of the last closed flux surface, which delimitates the plasma boundary. Perfectly straight lines mean that a very precise level of quasisymmetry is achieved. (Right) Poincaré plot showing a cross-section of the plasma where multiple nested flux surfaces are visible with no island chains.

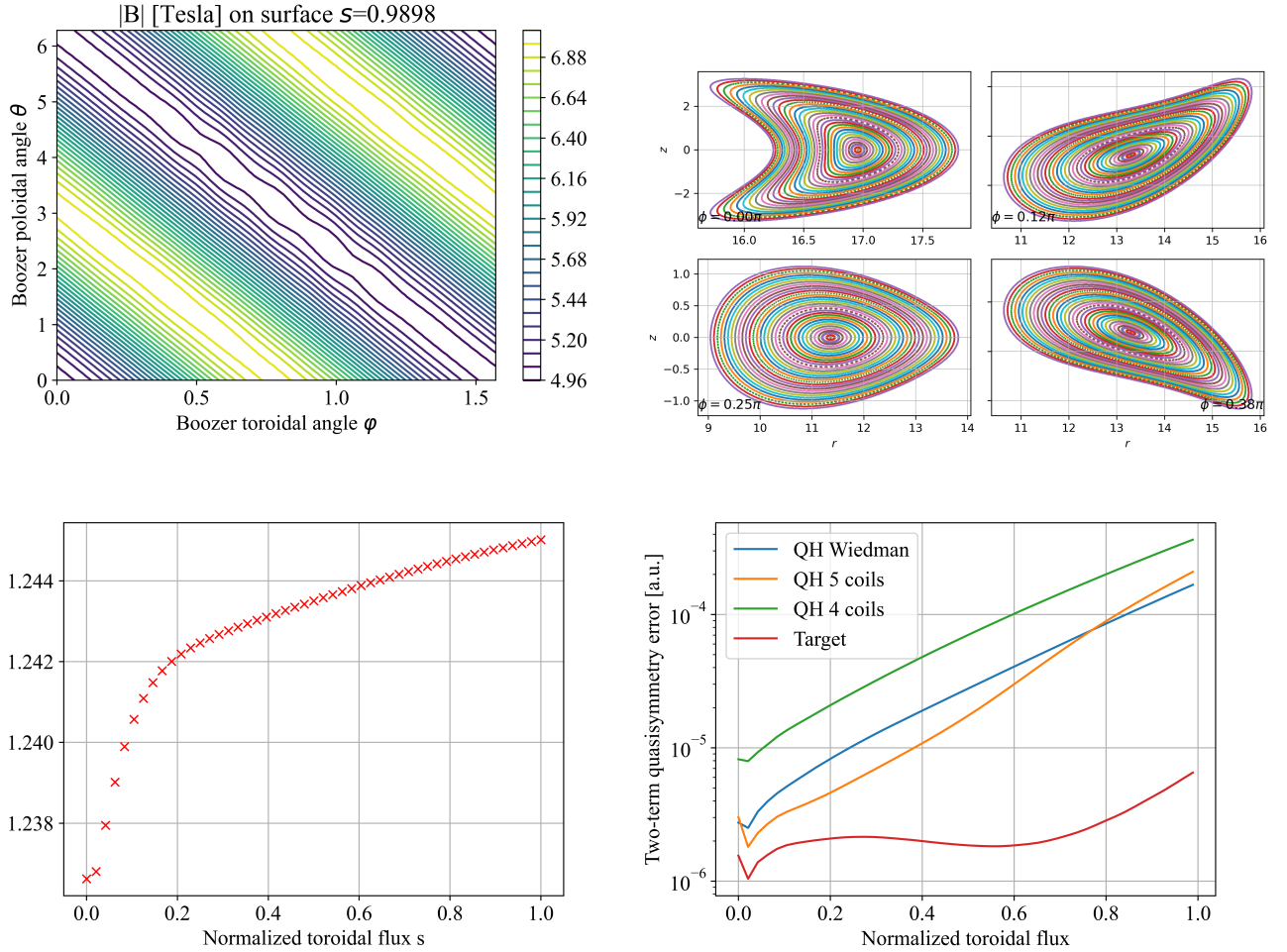


FIG. 8. (Top Left) Boozer plot for configuration #1 showing the quality of the quasi-helical symmetry of the last closed flux surface. Perfectly straight lines mean that a very precise level of quasisymmetry is achieved. (Top Right) Poincaré plot of configuration #1 showing a cross-section of the plasma where multiple nested flux surfaces are visible with no island chains and rotational transform profile of the configuration which matches the ideal profile. (Bottom Left) Rotational transform profile of configuration #1. (Bottom Right) QS profiles for the configurations #1, #2, Wiedman, and the original QH target plasma.

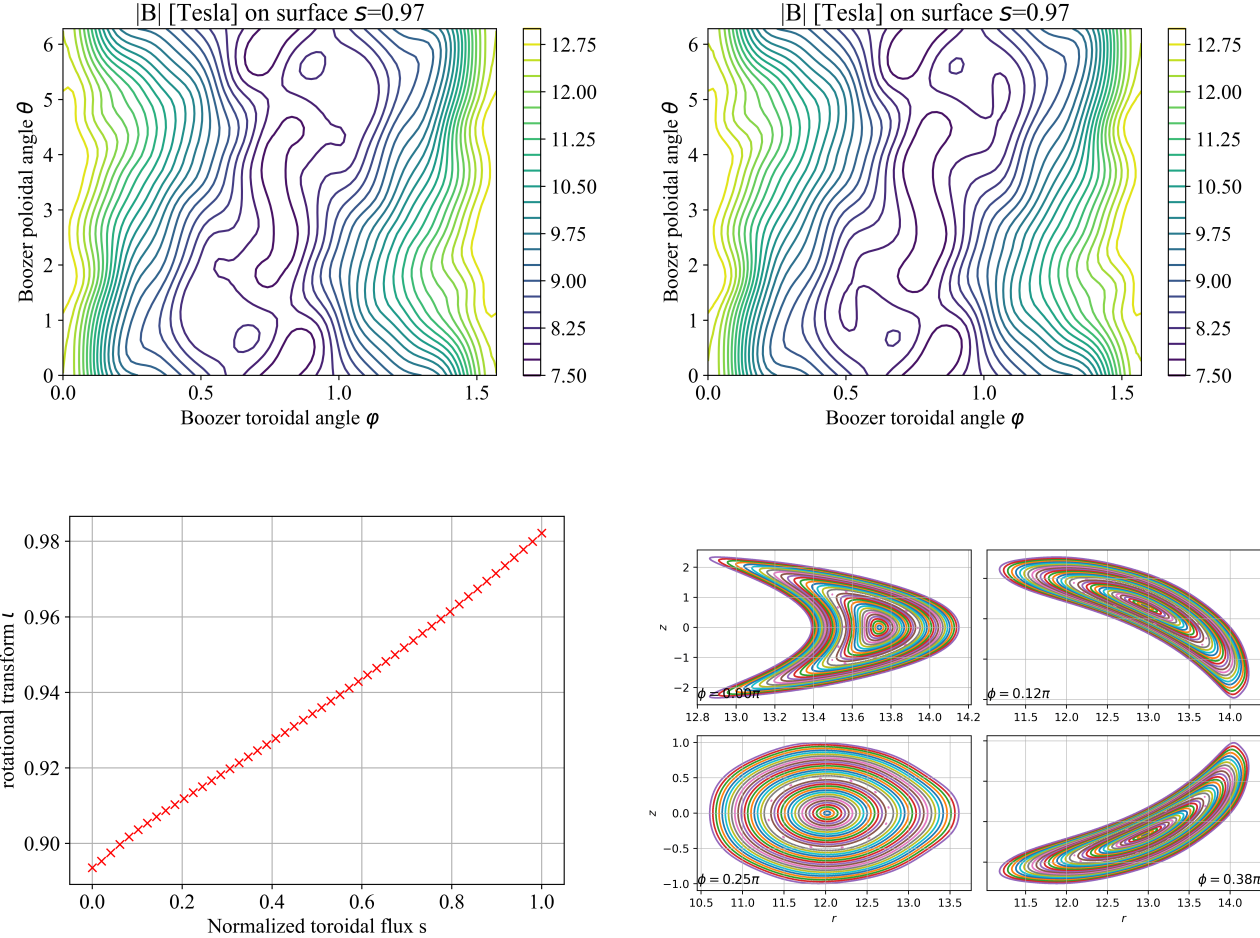


FIG. 9. (Top Left) Boozer plot of the #2 Stellaris configuration showing the quality of the quasi-isodynamic field generated by the coils (Top Right) Boozer plot of the target isodynamic-field of Stellaris. The coils appear to accurately capture the desired features of the boundary magnetic surface.(Bottom Left) Rotational transform profile of the #2 Stellaris configuration. (Bottom Right) Poincaré plots of the #2 configuration.

- [20] L. Fu, E. J. Paul, A. A. Kaptanoglu, and A. Bhattacharjee, Global stellarator coil optimization with quadratic constraints and objectives, *Nuclear Fusion* **65**, 026045 (2025).
- [21] M. Drevlak, Optimization of heterogenous magnet systems, *12th International Stellarator Workshop, Madison, WI* (1999).
- [22] N. Pomphrey, L. Berry, A. Boozer, A. Brooks, R. Hatcher, S. Hirshman, L.-P. Ku, W. Miner, H. Mynick, W. Reiersen, D. Strickler, and P. Valanju, Innovations in compact stellarator coil design, *Nuclear Fusion* **41**, 339 (2001).
- [23] D. J. Strickler, L. A. Berry, and S. P. H. and, Designing coils for compact stellarators, *Fusion Science and Technology* **41**, 107 (2002), <https://doi.org/10.13182/FST02-A206>.
- [24] T. Brown, J. Breslau, D. Gates, N. Pomphrey, and A. Zolfaghari, Engineering optimization of stellarator coils lead to improvements in device maintenance, in *2015 IEEE 26th Symposium on Fusion Engineering (SOFE)* (2015) pp. 1–6.
- [25] J. Lion, J.-C. Anglès, L. Bonauer, A. Bañón Navarro, S. Cadena Ceron, R. Davies, M. Drevlak, N. Foppiani, J. Geiger, A. Goodman, W. Guo, E. Guiraud, F. Hernández, S. Henneberg, R. Herrero, C. Hintze, H. Höchter, J. Jelonnek, F. Jenko, R. Jorge, M. Kaiser, M. Kubie, E. Lascas Neto, H. Laqua, M. Leoni, J. Lobsien, V. Maurin, A. Merlo, D. Middleton-Gear, M. Pascu, G. Plunk, N. Riva, M. Savtchouk, F. Sciortino, J. Schilling, J. Shimwell, A. Di Siena, R. Slade, T. Stange, T. Todd, L. Wegener, F. Wilms, P. Xanthopoulos, and M. Zheng, Stellaris: A high-field quasi-isodynamic stellarator for a prototypical fusion power plant, *Fusion Engineering and Design* **214**, 114868 (2025).
- [26] D. T. Anderson, J. M. Canik, C. C. Hegna, and C. M. Mowry, A comprehensive, unified baseline physics design for the type one energy stellarator fusion pilot power plant, ‘Infinity Two’, *Journal of Plasma Physics* **91**, e65 (2025).
- [27] D. Gates, S. Aslam, B. Berzin, P. Bonofiglio, A. Cote, D. Dudit, E. Flom, D. Fort, A. Koen, T. Kruger, S. Kumar, M. Martin, A. Ottaviano, S. Pasman, P. Romano, C. Swanson, L. Tang, E. Winkler, and R. Wu, Stellarator

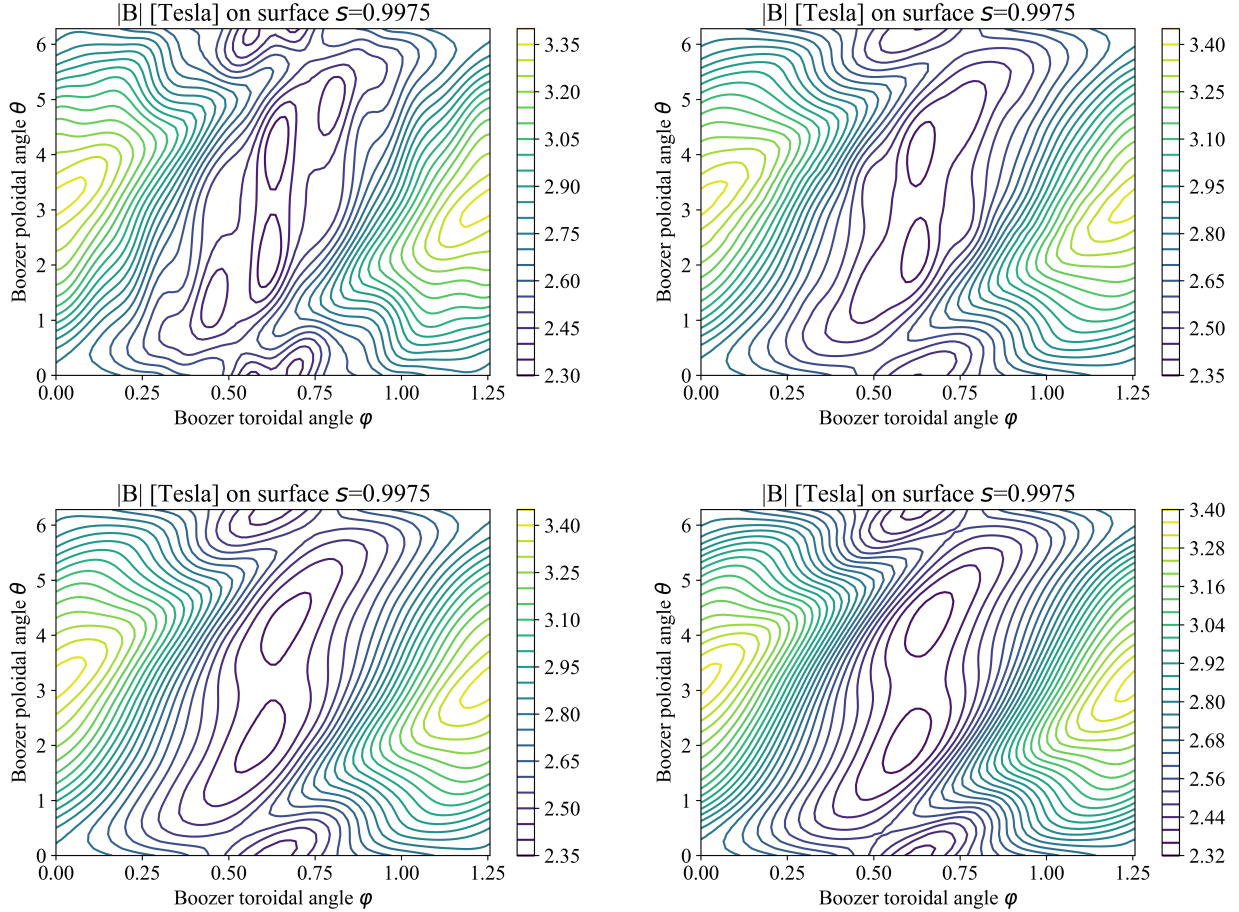


FIG. 10. Boozer plots of the four W7-X configurations presented in this work showing the quality of the omnigenous field generated by the coils: four coils per half field period (#1 Top Left), five coils per hfp with 45 m coil length and reduced forces (#2 Top Right), five coils per hfp with 43 m coil length and best field accuracy (#3 Bottom Left) and the target W7-X field in fixed-boundary (Bottom Right).

- fusion systems enabled by arrays of planar coils, *Nuclear Fusion* **65**, 026052 (2025).
- [28] F. Volpe, Renaissance Fusion Technologies, <https://renfusion.eu/technology> (2023), accessed: 1 October 2023.
  - [29] J. Miyazawa and T. Goto, Development of steady-state fusion reactor by Helical Fusion, *Physics of Plasmas* **30**, 050601 (2023), [https://pubs.aip.org/aip/pop/article-pdf/doi/10.1063/5.0145222/19997113/050601\\_1.5.0145222.pdf](https://pubs.aip.org/aip/pop/article-pdf/doi/10.1063/5.0145222/19997113/050601_1.5.0145222.pdf).
  - [30] A. Goodman, K. Camacho Mata, S. Henneberg, R. Jorge, M. Landreman, G. Plunk, H. Smith, R. Mackenbach, C. Beidler, and P. Helander, Constructing precisely quasi-isodynamic magnetic fields, *Journal of Plasma Physics* **89**, 905890504 (2023).
  - [31] D. W. Dudit, A. G. Goodman, R. Conlin, D. Panici, and E. Kolemen, Magnetic fields with general omnigenity, *Journal of Plasma Physics* **90**, 905900120 (2024).
  - [32] J. L. Velasco, I. Calvo, F. J. Escoto, E. Sánchez, H. Thienpondt, and F. I. Parra, Piecewise omnigenous stellarators, *Phys. Rev. Lett.* **133**, 185101 (2024).
  - [33] M. Landreman and P. J. Catto, Omnigenity as generalized quasisymmetry, *Physics of Plasmas* **19**, 056103 (2012), [https://pubs.aip.org/aip/pop/article-pdf/doi/10.1063/1.3693187/13988448/056103\\_1.online.pdf](https://pubs.aip.org/aip/pop/article-pdf/doi/10.1063/1.3693187/13988448/056103_1.online.pdf).
  - [34] A. G. Goodman, P. Xanthopoulos, G. G. Plunk, H. Smith, C. Nührenberg, C. D. Beidler, S. A. Henneberg, G. Roberg-Clark, M. Drevlak, and P. Helander, Quasi-isodynamic stellarators with low turbulence as fusion reactor candidates, *PRX Energy* **3**, 023010 (2024).
  - [35] R. Nies, E. J. Paul, D. Panici, S. R. Hudson, and A. Bhattacharjee, Exploration of the parameter space of quasisymmetric stellarator vacuum fields through adjoint optimisation, *Journal of Plasma Physics* **90**, 905900620 (2024).
  - [36] M. Landreman, Mapping the space of quasisymmetric stellarators using optimized near-axis expansion, *Journal of Plasma Physics* **88**, 905880616 (2022).
  - [37] M. Landreman, B. Medasani, F. Wechsung, A. Giuliani, R. Jorge, and C. Zhu, SIMSOPT: A flexible framework for stellarator optimization, *Journal of Open Source Software* **6**, 3525 (2021).
  - [38] P. Merkel, Solution of stellarator boundary value problems with external currents, *Nuclear Fusion* **27**, 867 (1987).

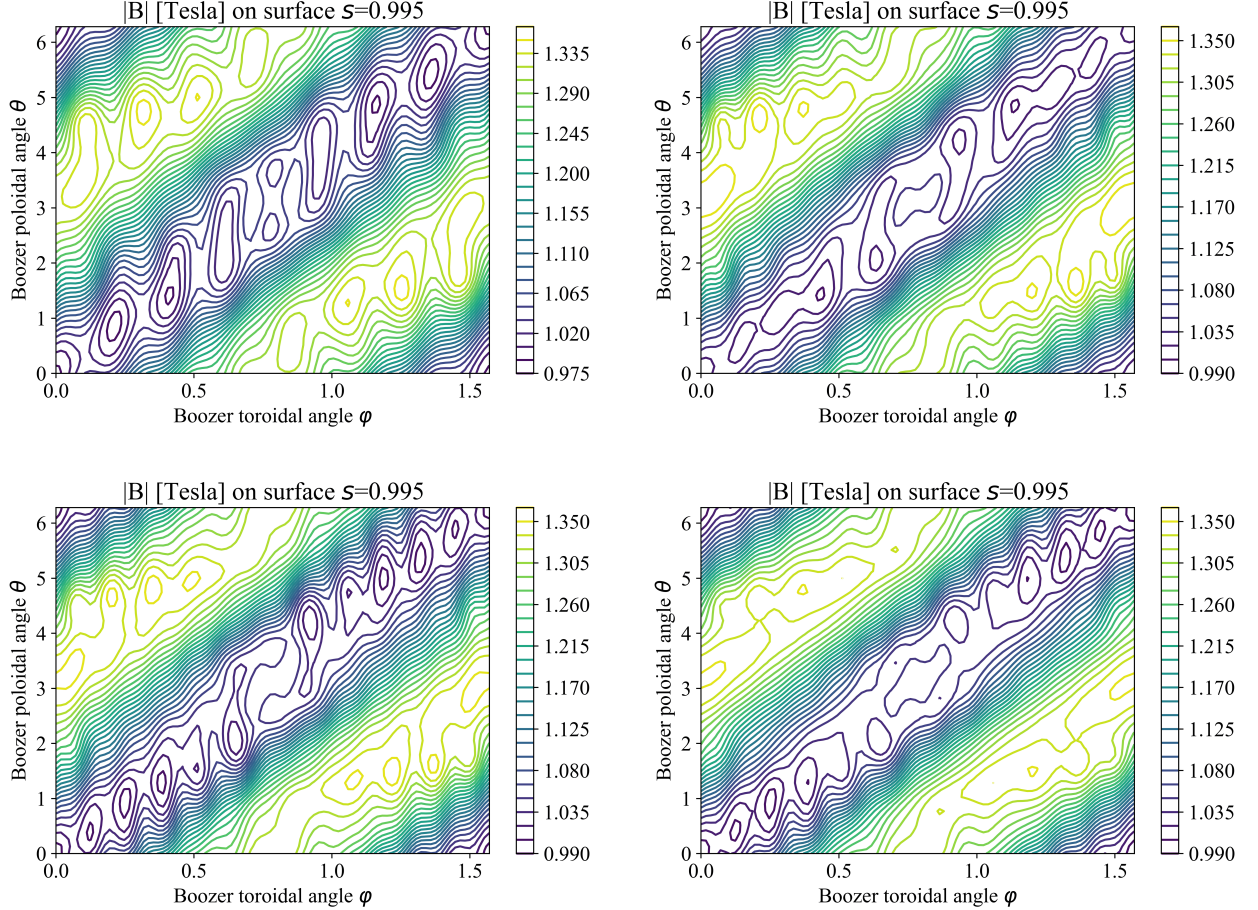


FIG. 11. Boozer plots of the four HSX configurations presented in this work showing the quality of the quasi-helically symmetric field generated by the coils: four coils per half field period (#1 Top Left), five coils per hfp (#2 Top Right), six coils per hfp (#3 Bottom Left) and the original HSX coil set (Bottom Right).

- [39] M. Landreman, An improved current potential method for fast computation of stellarator coil shapes, *Nuclear Fusion* **57**, 046003 (2017).
- [40] R. Conlin, P. Kim, D. W. Dutt, D. Panici, and E. Kolemen, Stellarator optimization with constraints, *Journal of Plasma Physics* **90**, 905900501 (2024).
- [41] A. R. Conn, N. I. M. Gould, and P. L. Toint, *Trust-Region Methods*, MPS/SIAM Series on Optimization (Society for Industrial and Applied Mathematics (SIAM), Philadelphia, PA, 2000).
- [42] J. Nocedal and S. J. Wright, *Numerical Optimization*, 2nd ed. (Springer Science & Business Media, 2006).
- [43] D. C. Liu and J. Nocedal, On the limited memory BFGS method for large scale optimization, *Mathematical programming* **45**, 503 (1989).
- [44] C. Zhu, S. R. Hudson, Y. Song, and Y. Wan, New method to design stellarator coils without the winding surface, *Nuclear Fusion* **58**, 016008 (2017).
- [45] A. A. Kaptanoglu, A. Wiedman, J. Halpern, S. Hurwitz, E. J. Paul, and M. Landreman, Reactor-scale stellarators with force and torque minimized dipole coils, *Nuclear Fusion* **65**, 046029 (2025).
- [46] Z. S. Hartwig, R. F. Vieira, B. N. Sorbom, R. A. Badcock, M. Bajko, W. K. Beck, B. Castaldo, C. L. Craighill, M. Davies, J. Estrada, *et al.*, VIPER: an industrially scalable high-current high-temperature superconductor cable, *Superconductor Science and Technology* **33**, 11LT01 (2020).
- [47] Z. Zhao, P. Moore, and L. Chiesa, Structural modeling of REBCO VIPER cable for high-field magnet applications, *IEEE Transactions on Applied Superconductivity* **32**, 1 (2022).
- [48] N. Riva, R. Granetz, R. Vieira, A. Hubbard, A. Pfeiffer, P. Harris, C. Chamberlain, Z. Hartwig, A. Watterson, D. Anderson, *et al.*, Development of the first non-planar REBCO stellarator coil using VIPER cable, *Superconductor Science and Technology* **36**, 105001 (2023).
- [49] S. Hurwitz, M. Landreman, and T. M. Antonsen, Efficient calculation of the self-magnetic field, self-force, and self-inductance for electromagnetic coils, *IEEE Transactions on Magnetics* **60**, 1 (2024).
- [50] R. Robin and F. A. Volpe, Minimization of magnetic forces on stellarator coils, *Nuclear Fusion* **62**, 086041 (2022).

- [51] S. Guinchard, S. R. Hudson, and E. J. Paul, Including the vacuum energy in stellarator coil design, *Plasma Physics and Controlled Fusion* **67**, 035028 (2025).
- [52] S. Hurwitz, M. Landreman, P. Huslage, and A. Kapitanoglu, Electromagnetic coil optimization for reduced Lorentz forces, *Nuclear Fusion* **65**, 056044 (2025).
- [53] F. Najmabadi, A. R. Raffray, S. I. Abdel-Khalik, L. Bromberg, L. Crosatti, L. El-Guebaly, P. R. Garabedian, A. A. Grossman, D. Henderson, A. Ibrahim, T. Ihli, T. B. Kaiser, B. Kiedrowski, L. P. Ku, J. F. Lyon, R. Maingi, S. Malang, C. Martin, T. K. Mau, B. Merrill, R. L. Moore, R. J. P. Jr., D. A. Petti, D. L. Sadowski, M. Sawan, J. H. Schultz, R. Slaybaugh, K. T. Slattery, G. Sviatoslavsky, A. Turnbull, L. M. Waganer, X. R. Wang, J. B. Weathers, P. Wilson, J. C. W. III, M. Yoda, and M. Zarnstorff, The ARIES-CS Compact Stellarator Fusion Power Plant, *Fusion Science and Technology* **54**, 655 (2008).
- [54] D. Spong, J. Harris, A. Ware, S. Hirshman, and L. Berry, Shear flow generation in stellarators—configurational variations, *Nuclear Fusion* **47**, 626 (2007).
- [55] A. Wiedman, S. Buller, and M. Landreman, Coil optimization for quasi-helically symmetric stellarator configurations, *Journal of Plasma Physics* **90**, 905900307 (2024).
- [56] P. Helander and J. Nührenberg, Bootstrap current and neoclassical transport in quasi-isodynamic stellarators, *Plasma Physics and Controlled Fusion* **51**, 055004 (2009).
- [57] P. Helander, Theory of plasma confinement in non-axisymmetric magnetic fields, *Reports on Progress in Physics* **77**, 087001 (2014).
- [58] H. E. Mynick, N. Pomphrey, and P. Xanthopoulos, Optimizing stellarators for turbulent transport, *Phys. Rev. Lett.* **105**, 095004 (2010).
- [59] J. Proll, G. Plunk, B. Faber, T. Görler, P. Helander, I. McKinney, M. Pueschel, H. Smith, and P. Xanthopoulos, Turbulence mitigation in maximum-J stellarators with electron-density gradient, *Journal of Plasma Physics* **88**, 905880112 (2022).
- [60] Helander, P. and Geiger, J. and Maaßberg, H., On the bootstrap current in stellarators and tokamaks, *Physics of Plasmas* **18**, 092505 (2011).
- [61] C. Beidler, G. Grieger, F. Herrnegger, E. Harmeyer, J. Kisslinger, W. Lotz, H. Maassberg, P. Merkel, J. Nuhrenberg, F. Rau, *et al.*, Physics and engineering design for Wendelstein VII-X, *Fusion Technology; (USA)* **17:1** (1990).
- [62] T. S. Pedersen, M. Otte, S. Lazerson, *et al.*, Confirmation of the topology of the Wendelstein 7-X magnetic field to better than 1:100,000, *Nature Communications* **7**, 13493 (2016).
- [63] S. P. Gerhardt, J. N. Talmadge, J. M. Canik, and D. T. Anderson, Measurements and modeling of plasma flow damping in the Helically Symmetric eXperiment, *Physics of Plasmas* **12**, 056116 (2005), [https://pubs.aip.org/aip/pop/article-pdf/doi/10.1063/1.1876293/13509317/056116\\_1\\_online.pdf](https://pubs.aip.org/aip/pop/article-pdf/doi/10.1063/1.1876293/13509317/056116_1_online.pdf).
- [64] J. M. Canik, D. T. Anderson, F. S. B. Anderson, C. Clark, K. M. Likin, J. N. Talmadge, and K. Zhai, Reduced particle and heat transport with quasisymmetry in the Helically Symmetric Experiment, *Physics of Plasmas* **14**, 056107 (2007), [https://pubs.aip.org/aip/pop/article-pdf/doi/10.1063/1.2709862/13887817/056107\\_1\\_online.pdf](https://pubs.aip.org/aip/pop/article-pdf/doi/10.1063/1.2709862/13887817/056107_1_online.pdf).